(1)

KrF-laser-pumped metal vapor lasers

H. Yoshida

CONTENTS

ABSTRACT

ABSTRACT

New laser oscillations of iron and tantalum atoms have been observed for the first time by author with the aid of optically pumped Fe and Ta vapor plasmas, respectively. The vapor plasma is produced by irradiating a metal plate with a pulsed Nd:YAG laser, which is optically pumped by a KrF excimer laser.

An Fe vapor laser oscillation has been first observed on three lines in an ultraviolet region (299.951, 303.164 and 304.043 nm), and on two lines in a visible region (532.418 and 562.455 nm). Output characteristics of the ultraviolet and visible Fe vapor lasers have been investigated experimentally. The maximum output energies of the ultraviolet and visible Fe lasers are 1.08 μJ/pulse and 135.3 nJ/pulse, respectively. Under optimum lasing conditions, the optical gains at 299.951, 303.164, 304.043, 532.418 and 562.455 nm are 1.53, 1.04, 1.77, 0.66 and 0.41 /cm, respectively.

In order to elucidate the oscillation mechanisms of the Fe vapor lasers, a dynamics of the laser-induced Fe vapor plasma has been investigated experimentally. Population densities of Fe atoms, an absolute gas temperature and an electron density have been measured by using the hook method, the Boltzmann plot method and the Saha ionization theory, respectively. On the basis of the experimental results, a clear physical interpretation is given for the output characteristics of the Fe vapor lasers. A set of rate equations for the formations of the laser upper and lower states is calculated, and the oscillation mechanisms of the Fe vapor laser are elucidated.

A Ta vapor laser oscillation has also been first observed on five lines in an ultraviolet region (292.519, 322.732, 328.087, 330.438 and 351.361 nm). Output characteristics of the Ta vapor lasers have been investigated experimentally, and the maximum output energy of 160 nJ/pulse is obtained. Under an optimum lasing condition, the optical gains at 292.519, 322.732, 328.087, 330.438 and 351.361 nm are 0.35, 0.24, 0.09, 0.09 and 0.20 /cm, respectively.

INTRODUCTION

INTRODUCTION

Many metallic materials are used in a nuclear power plant, whose component is strictly controlled to keep a high degree of safety and reliability[1]. However, metallic materials used for a nuclear reactor coolant system are corroded by a deposition of trace metallic elements in materials into a cooling water[2,3]. The deposited metallic elements cause an increase in a radiation quantity in the plant, because they are radioactivated[4]. For a preventive maintenance of the reactor coolant system, a concentration of metallic elements in the cooling water is measured, and this maintenance work takes many hours[5]. In order to improve the safety and working efficiency of the preventive maintenance, a development of techniques for measuring the metallic elements with a remote sensibility and a high sensitivity is desired.

On the other hand, extensive efforts have recently been devoted to researches into a spectroscopic analysis and a separation of elements by making use of lasers[6-8]. These techniques using a laser have a remote sensibility, a high sensitivity and a selectivity, which are very profitable for applications to bad environmental conditions[9,10]. A dye laser is a candidate for a light source of these techniques due to a tunability in a wide wavelength range. These techniques require an accurate and stable spectral control of the light source. The dye laser is not necessarily suitable for the light source of these techniques, because the accurate and stable spectral control of the dye laser is critical[11,12]. The purpose of this study is to develop a novel metal vapor laser with fixed individual wavelengths of the metallic element which is a measuring object in the nuclear power plant.

An Fe atom is one of important measuring objects in the nuclear power plant, because Fe atoms in materials such as a stainless steel deposit into the cooling water and they are radioactivated[5,13]. Therefore, a development of an Fe vapor laser with a fixed individual wavelength of the Fe atom is desired as a light source for a spectroscopic analysis or a separation of Fe atoms in the mixture of many metallic elements. As a result of this study, the Fe vapor lasers have been first obtained at the wavelengths of 299.951, 303.164, 304.043, 532.418 and 562.455 nm.

In a nuclear reactor, a concentration of Ta atoms in materials such as a niobium steel is strictly controlled, because the Ta atom has a high neutron absorption cross section (1.1 barn)[14,15]. Therefore, a development of a Ta vapor laser with a fixed individual wavelength of the Ta atom has been desired as a light source for a spectroscopic analysis or a separation of Ta atoms in the mixture of many metallic elements. As a result of this study, the Ta vapor lasers have been first

obtained at the wavelengths of 292.519, 322.732, 328.087, 330.438 and 351.361 nm.

The Ta metal has a high melting-point (3263 K)[16]. As a usual method to obtain metal vapor, a heating method by means of the furnace or discharge has been used[17-19]. However, in the usual methods, it is not easy to obtain a sufficient amount of metal vapor from high melting metals such as the Ta metal. In this study, a Ta vapor is produced by irradiating a Ta metal plate with a pulsed Nd:YAG laser. It is suggested that this vaporization method is applicable to high melting metals. An Fe vapor is obtained by the same vaporization method as the Ta vapor. Fe and Ta vapor are optically pumped by a KrF excimer laser. The KrF laser has high power, fast rise time and wide linewidth[20], which is suitable for an optical pumping source to obtain population inversion on a laser transition in metal vapor. These metal vapor lasers offer various wavelengths by changing the metal plate in the same device.

Chapter 1 is concerned with an experimental study of output characteristics of the KrF-laser-pumped Fe vapor laser. In order to elucidate oscillation mechanisms of the Fe vapor laser, a dynamics of the Fe vapor plasma has been investigated experimentally. Population densities of Fe atoms, an absolute gas temperature and an electron density have been measured by using the hook method, the Boltzmann plot method and the Saha ionization theory, respectively[21-27]. On the basis of the experimental results, a clear physical interpretation is given for the output characteristics of the Fe vapor laser. A set of rate equations for the formations of the laser upper and lower states is calculated, and the oscillation mechanisms of the Fe vapor laser are discussed.

Chapter 2 is concerned with an experimental study of output characteristics of the KrF-laser-pumped Ta vapor laser. An output energy of the Ta vapor laser has been measured as a function of the pulsed Nd:YAG laser energy for vaporization and the KrF laser energy for optically pumping. A maximum horizontal length of the Ta vapor plasma has been measured as a function of a He buffer gas pressure and an irradiating delay time between the YAG laser and the KrF laser. Under an optimum lasing condition, optical gains of the Ta vapor lasers has been measured.

CHAPTER 1

Laser action of optically pumped Fe vapor

1-1. Fe vapor laser

A laser oscillation of Fe atom was first obtained in infrared region (at 6.8 and 8.5 μm) by electrical dissociation of metal complexes in 1977.[28] Thereafter, laser oscillations of Fe atom in from visible to ultraviolet region (at 563, 558, 540, 453, 395, 385 and 360 nm) were obtained by a pulsed excitation of Fe vapor or photo-dissociation of metal complexes in 1978.[29,30]

A novel metal vapor laser action has been studied by making use of an optically pumping technique by author. A laser oscillation of Fe I atom has been first obtained by optically pumping Fe vapor. The Fe vapor is produced by irradiating an Fe metal plate with a pulsed Nd:YAG laser, and Fe atoms in the vapor are optically pumped by a KrF excimer laser at about 248 nm. New laser actions of Fe atom are observed on five lines at 299.951, 303.164, 304.043, 532.418 and 562.455 nm.

Figure 1-1 shows energy levels pertinent to the optically pumped Fe vapor laser.[31-33] This laser has two optical pumping mechanisms: (1)ground-state Fe [$3d^64s^2\ ^5d_4$] atoms are excited to the laser upper level [$3d^64s(^4D)4p\ ^5F^o_5$] by absorbing light at 248.327 nm, (2)Fe [$3d^64s^2\ ^5D_1$] atoms are excited to the laser upper level [$3d^64s(^4D)4p\ ^5F^o_1$] by absorbing light at 248.419 nm. The Doppler half-width on these absorption lines at the melting-point (1808 K) is calculated to be 1.01×10^{-3} nm.

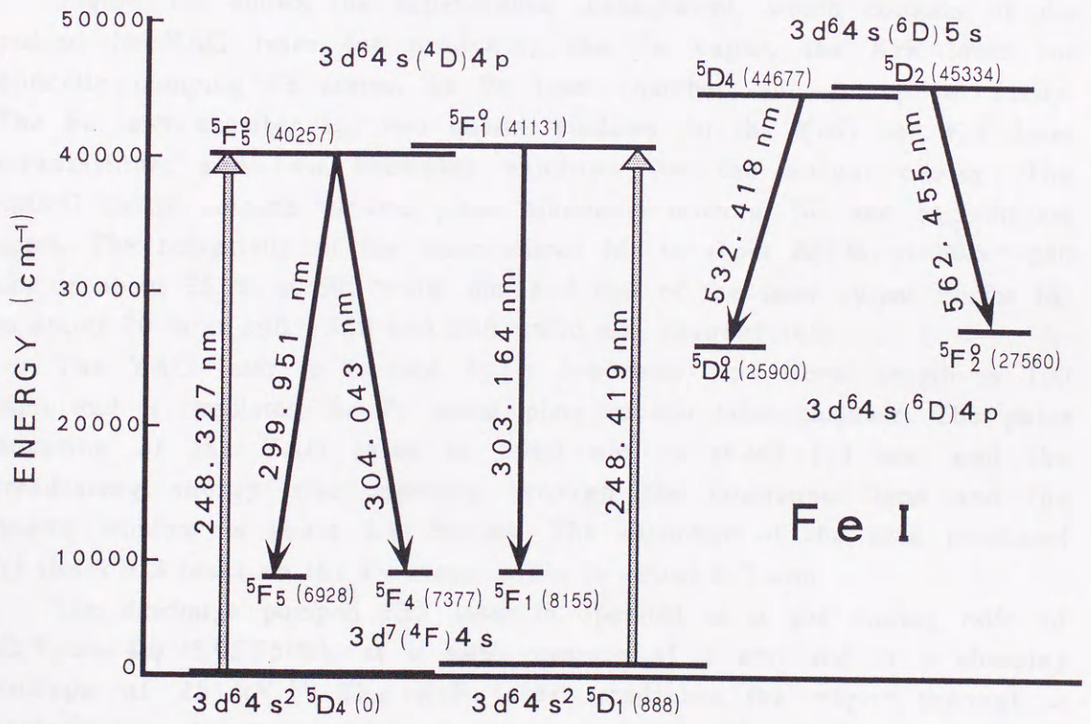

FIG. 1-1. Energy levels of Fe I pertinent to the Fe vapor laser.

The upper states [$3d^6 4s(^4D)4p\ ^5F^\circ_5$ and $3d^6 4s(^4D)4p\ ^5F^\circ_1$] of the ultraviolet laser lines at 299.951, 303.164 and 304.043 nm are optically pumped by the KrF laser. The upper states of the visible laser lines at 532.418 and 562.455 nm can be not directly pumped by the KrF laser.

Table 1-1 lists the wavelengths, transitions and Einstein transition probabilities of the Fe vapor laser lines.[31-33]

TABLE 1-1. Laser transition of an Fe atom. (λ (nm):wavelength, A ($10^8\ s^{-1}$) and B ($10^{20}\ m^3\ J^{-1}\ s^{-2}$):Einstein transition probability, τ (ns):lifetime)

λ	Upper level - Lower level	A	B
299.951	$3d^6\ 4s(^4D)4p\ ^5F^\circ_5$ - $3d^7\ (^4F)4s\ ^5F_5$	0.47 (τ =21)	0.762
304.043	$3d^6\ 4s(^4D)4p\ ^5F^\circ_5$ - $3d^7\ (^4F)4s\ ^5F_4$	0.23 (τ =43)	0.388
303.164	$3d^6\ 4s(^4D)4p\ ^5F^\circ_1$ - $3d^7\ (^4F)4s\ ^5F_1$	1.20 (τ =8)	2.009
532.418	$3d^6\ 4s(^6D)5s\ ^5D_4$ - $3d^6\ 4s(^6D)4p\ ^5D^\circ_4$	0.70 (τ =14.3)	6.347
562.455	$3d^6\ 4s(^6D)5s\ ^5D_2$ - $3d^6\ 4s(^6D)4p\ ^5F^\circ_2$	0.22 (τ =45.5)	2.352

1-2. Experimental methods

Figure 1-2 shows the experimental arrangement, which consists of the pulsed Nd:YAG laser for producing the Fe vapor, the KrF laser for optically pumping Fe atoms, an Fe laser chamber, and an optical cavity. The Fe laser chamber has two quartz windows for the YAG and KrF laser irradiations, and two Brewster windows for the output cavity. The optical cavity consists of two plane aluminum mirrors, M_1 and M_2, 30 cm apart. The reflectivity of the laser mirror M_1 is about 88 % at 290 ~390 nm or about 85 % at 500 ~600 nm, and that of the laser output mirror M_2 is about 70 % at 290~350 and 500~600 nm, respectively.

The YAG laser is focused by a condenser lens (focal length is 100 mm) and it irradiates the Fe metal plate in the laser chamber. The pulse duration of the YAG laser at 1060 nm is about 1.3 ms, and the irradiating energy after passing through the condenser lens and the quartz window is about 2.0 J/pulse. The diameter of the area irradiated by the YAG laser on the Fe metal plate is about 0.7 mm.

The discharge pumped KrF laser is operated at a gas mixing ratio of $Kr:F_2:Ne=4:0.25:95.75(\%)$, at a total pressure of 3 atm and at a charging voltage of 25 kV.[20] The KrF laser irradiates the vapor through a rectangular slit (about 10 mm in width × 25 mm in high). The irradiating energy of the KrF laser in the laser chamber after passing

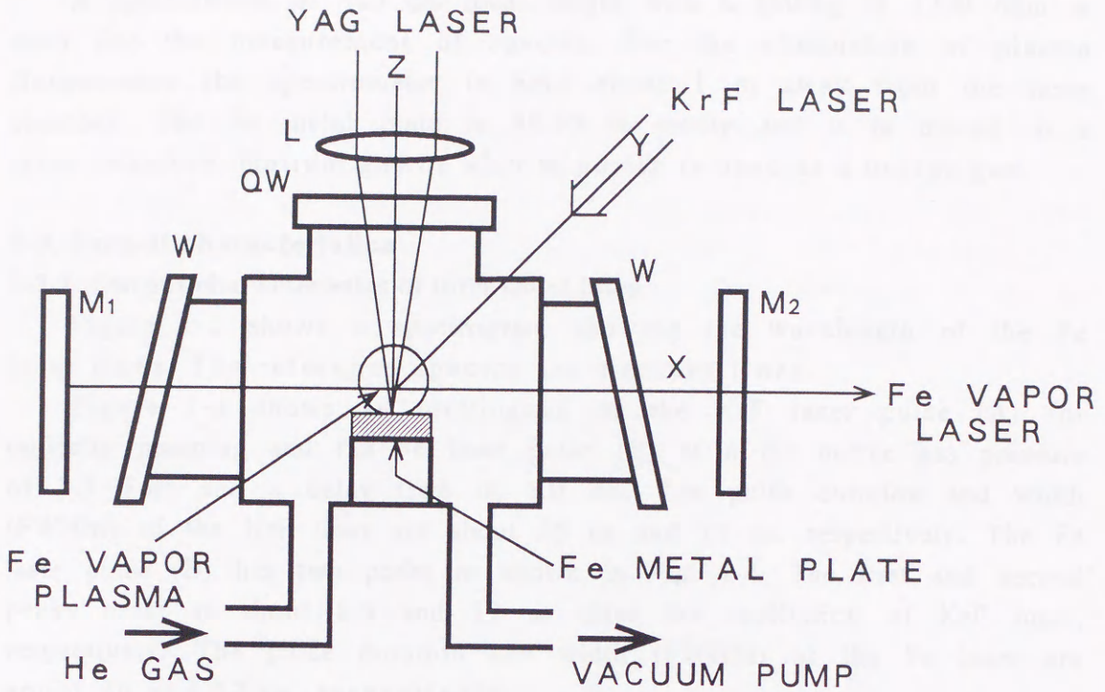

FIG. 1-2. Schematic diagram of Fe vapor laser.
(QW:quartz window, W:laser output window, M_1 :laser mirror, M_2 :laser output mirror, L:condenser lens)

through the quartz window is 34.0 $\pm$1.2 mJ/pulse. The KrF laser has a center wavelength at 248.4 nm and linewidth of 0.4 nm[34] (full width at half maximum: FWHM), which encloses the Fe absorption lines at 248.327 and 248.419 nm.

In order to measure the time variation of the Fe laser output power, the KrF laser is operated by a trigger pulse with a predetermined delay time. The delay time is determined by observing the signals of the two laser lights displayed on an oscilloscope. Hereafter, the irradiating delay time between the YAG and KrF laser is simply represented as the delay time.

In order to measure the maximum horizontal length of the Fe laser medium, the KrF laser irradiates the vapor with a certain delay time, and then an image of its fluorescence is photographed through an optical band-pass filter (in the vicinity of 300 nm). The length of the laser medium is measured from the profile of fluorescence obtained on the photograph.

An optical attenuator (neutral density filter) is inserted in the optical cavity for measuring the optical gains of the Fe vapor lasers, and the transmittance of the attenuator at the threshold for lasing is measured.[35]

A spectrometer of 100 cm focal length with a grating of 1200 /mm is used for the measurement of spectra. For the elimination of plasma fluorescence the spectrometer is held about 1 m away from the laser chamber. The Fe metal plate is 99.99 % purity and it is placed in a laser chamber. Helium gas of 99.9 % purity is used as a buffer gas.

1-3. Output characteristics

1-3-1. Output characteristics of ultraviolet lines

Figure 1-3 shows a spectrogram showing the wavelength of the Fe laser lines. The reference spectra are mercury lines.

Figure 1-4 shows an oscillogram of the KrF laser pulse (A) for optically pumping and the Fe laser pulse (B) at a He buffer gas pressure of 3.3 Torr and a delay time of 1.0 ms. The pulse duration and width (FWHM) of the KrF laser are about 25 ns and 11 ns, respectively. The Fe laser pulse (B) has two peaks as shown in Fig. 1-4. The first and second peaks exist at about 8.5 and 12 ns after the oscillation of KrF laser, respectively. The pulse duration and width (FWHM) of the Fe laser are about 20 and 12 ns, respectively.

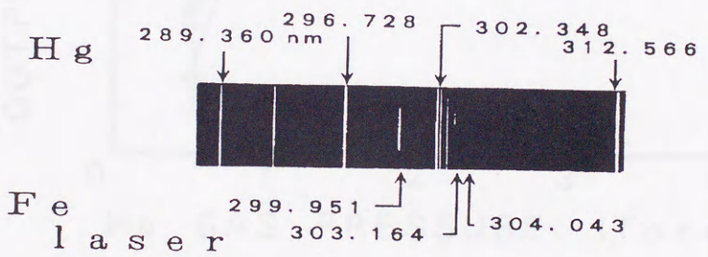

FIG. 1-3. Spectrogram showing the wavelength of the Fe laser lines.

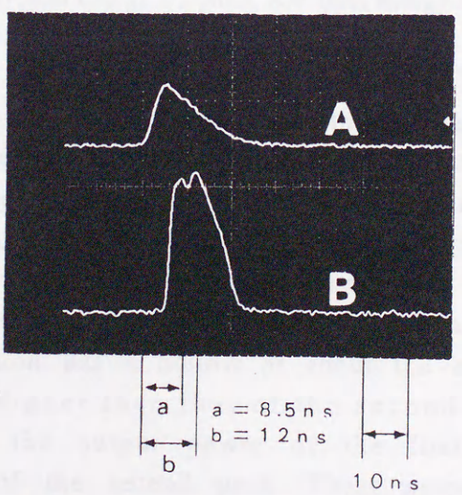

FIG. 1-4. Oscillogram of the KrF laser pulse (A) and the Fe laser pulse(B).

Figure 1-5 shows the dependence of the Fe laser output power of the first and second peaks on the He buffer gas pressure. The Fe laser output power increases with increasing the He buffer gas pressure, reaches a maximum at 3.3 Torr and then decreases. In the low pressure region, the output power of the first peak is higher than that of the second peak. On the other hand, in the high pressure region, the output power of the second peak is higher than that of the first peak. The maximum output powers of the first and second peaks are about 66 and 95 W, respectively.

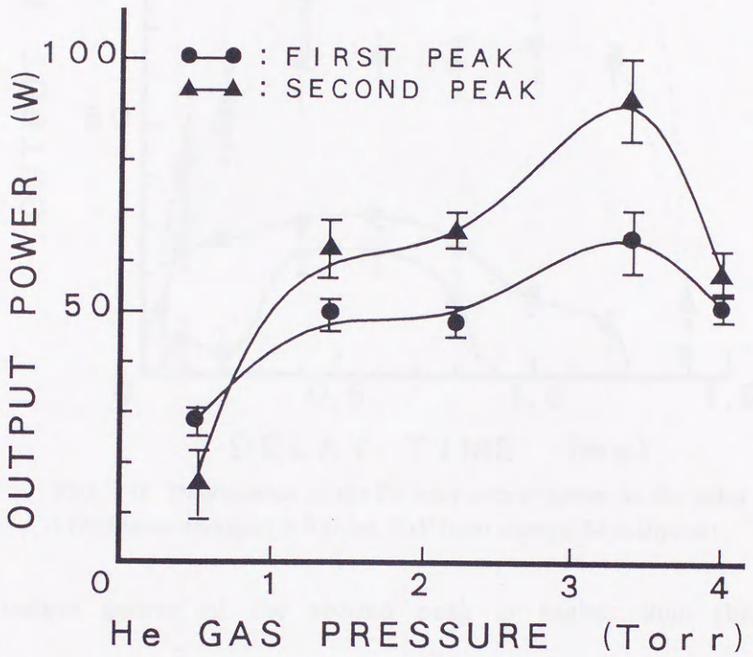

FIG. 1-5. Dependence of the Fe laser output power on the He buffer gas pressure.
(YAG laser energy:2 J/pulse, KrF laser energy:34 mJ/pulse, delay time:1.0 ms)

Figure 1-6 shows the dependence of the Fe laser output power on the delay time. An Fe laser oscillation is observed after about 0.05 ms. At 0.6 Torr, the output power of the first peak increases with the delay time, reaches a maximum at about 0.6 ms and then decreases monotonously to 1.25 ms. The output power of the second peak increases with the delay time, reaches a maximum at about 0.6 ms and then decreases to 8.5 ms, and the time variation has a hollow at about 0.2 ms. The output power of the first peak is higher than that of the second peak.

At 3.3 Torr, the output power of the first peak shows a similar tendency as that of the second peak. These output powers increase with the delay time, reach a maximum at about 1.0 ms and then decrease to 1.4

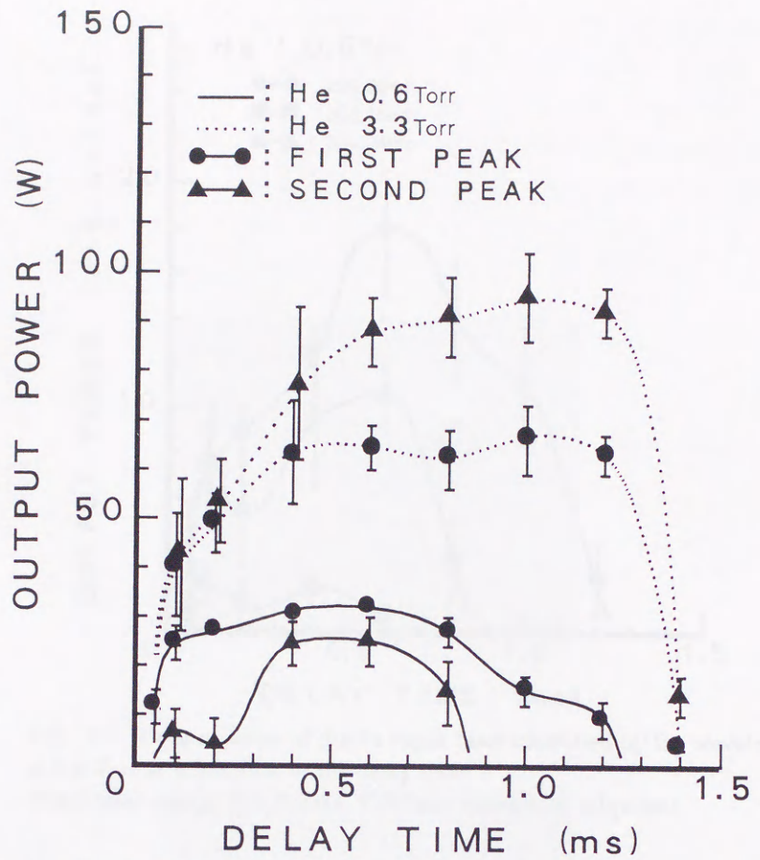

FIG. 1-6. Dependence of the Fe laser output power on the delay time.
(YAG laser energy:2.0 J/pulse, KrF laser energy:34 mJ/pulse)

ms. The output power of the second peak is higher than that of the first peak.

The output power of the Fe laser classified by the wavelengths (299.95, 303.16 and 304.04 nm) is shown in Figs. 1-7 and 1-8 as a function of the delay time. In Fig. 1-7, at 0.6 Torr, the output power of the 299.95 nm line increases with the delay time, reaches a maximum at 0.6 ms and then decreases to about 1.25 ms. The output power of the 304.04 nm line increases with the delay time, reaches a maximum at 0.6 ms and then decreases to 8.5 ms, and the time variation has a hollow at about 0.2 ms. The output power of the 303.16 nm line shows a similar tendency as that of the 304.04 nm line. The output power of the 299.95 nm line is higher than that of the 304.04 nm line, and that of the 303.16 nm line is very small.

In Fig. 1-8, at 3.3 Torr, the output powers of the 299.95 and 304.04 nm lines increases with the delay time, reach a maximum at about 1.0 ms and then decrease. The time variation has a hollow at about 0.6 ms. The laser light of the 303.16 nm line is not observed. The output power of the 304.04 nm line is higher than that of the 299.95 nm line.

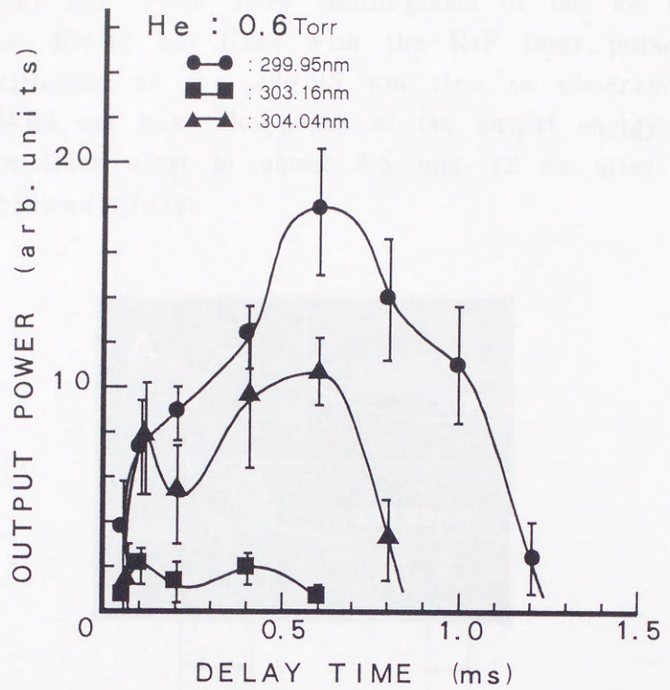

FIG. 1-7. Output power of the Fe vapor laser classified by the wavelength at 0.6 Torr as a function of the delay time.
(YAG laser energy:2.0 J/pulse, KrF laser energy:34 mJ/pulse)

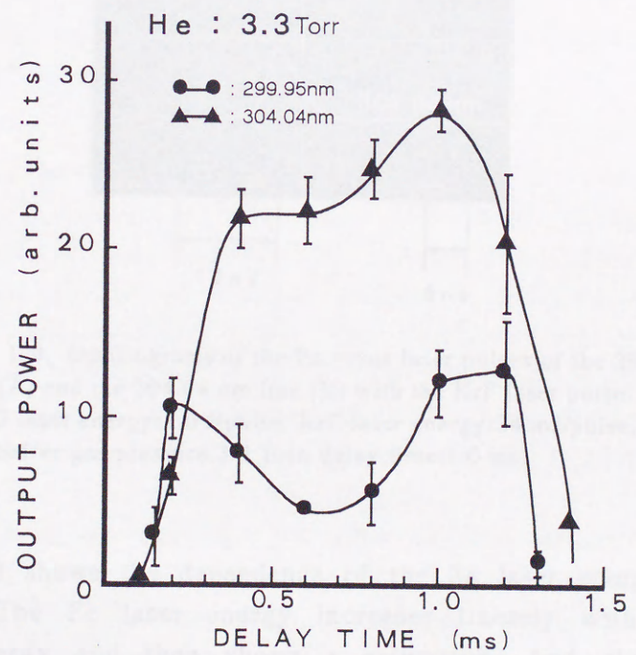

FIG. 1-8. Output power of the Fe vapor laser classified by the wavelength at 3.3 Torr as a function of the delay time.
(YAG laser energy:2.0 J/pulse, KrF laser energy:34 mJ/pulse)

Figure 1-9(a) and 1-9(b) show oscillograms of the Fe laser pulses of the 299.95 and 304.04 nm lines with the KrF laser pulse, respectively. The laser oscillation of the 299.95 nm line is observed earlier than that of the 304.04 nm line. The peaks of the output energy of the 299.95 and 304.04 nm lines exist at about 8.5 and 12 ns after the KrF laser oscillation, respectively.

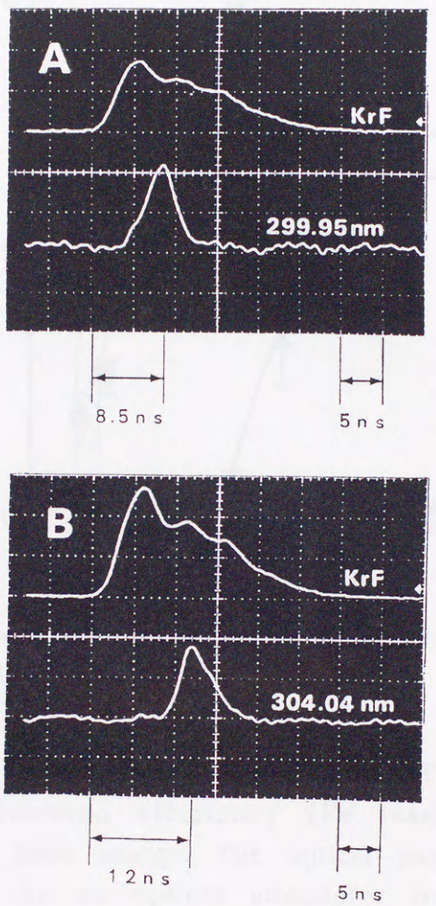

FIG. 1-9. Oscillograms of the Fe vapor laser pulses of the 299.95 nm line (A) and the 304.04 nm line (B) with the KrF laser pulse.
(YAG laser energy:2.0 J/pulse, KrF laser energy:34 mJ/pulse,
He buffer gas pressure:3.3 Torr, delay time:1.0 ms)

Figure 1-10 shows the dependence of the Fe laser energy on the YAG laser energy. The Fe laser energy increases linearly with increasing the YAG laser energy and then shows a saturation. And also the Fe laser energy increases with increasing the KrF laser energy. When the YAG laser energy is 2.0 J/pulse and the KrF laser energy is 34 mJ/pulse, the maximum Fe laser energy of 1.08 μJ/pulse is obtained.

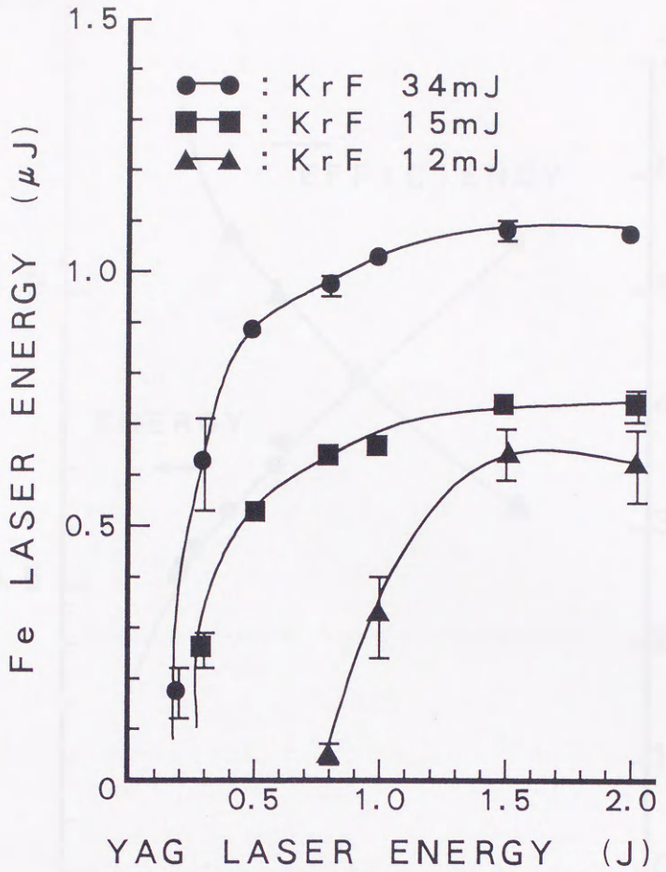

FIG. 1-10. Dependence of the Fe vapor laser energy on the YAG laser energy. (He buffer gas pressure:3.3 Torr, delay time:1.0 ms)

Figure 1-11 shows the dependences of the Fe laser energy and the optical energy conversion efficiency (Fe laser energy / KrF laser energy) on the KrF laser energy. The optical pumping energy (KrF laser energy) is changed by an optical attenuator inserted between the Fe laser chamber and the KrF laser. The Fe laser energy increases with increasing the KrF laser energy. The optical energy conversion efficiency decreases with increasing the KrF laser energy. A maximum value of 6.5×10^{-3} (%) is obtained at the KrF laser energy of 10 mJ/pulse.

Figure 1-12 shows the time variation of the horizontal length of the Fe laser medium at a vertical distance of 12 mm from the surface of the Fe metal plate. The Fe laser medium expands rapidly and then shows a plateau. The length of the Fe laser medium becomes shorter with increasing the He gas pressure. The length of the Fe laser medium significantly affects the laser output, because it is equal to the gain length.

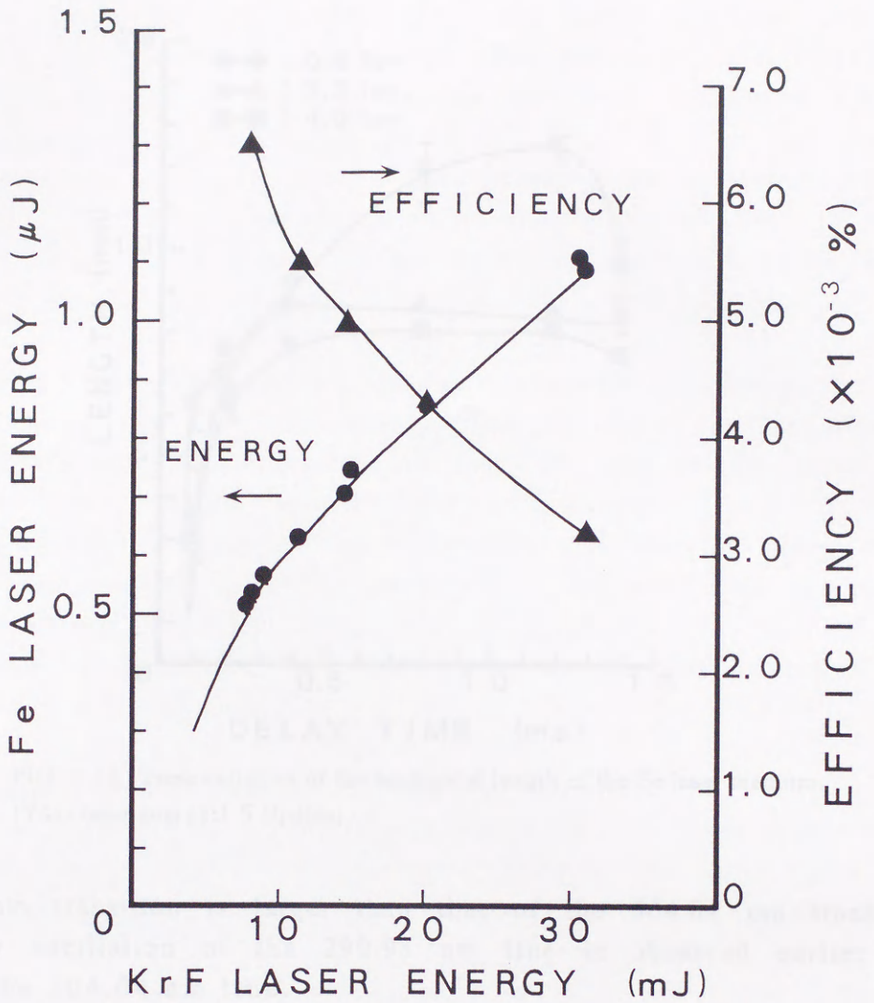

FIG. 1-11. Fe vapor laser energy and optical energy conversion efficiency as a function of the KrF laser energy.
(YAG laser energy:2.0 J/pulse, He buffer gas pressure:3.3 Torr, delay time:1.0 ms)

Under the optimum lasing condition (at the He buffer gas pressure of 3.3 Torr and the delay time of 1.0 ms), the measured optical gains at 299.95 and 304.04 nm are 1.53 and 1.77 /cm, respectively.

In comparison of Figs. 1-4 and 1-9, it is confirmed that the first and second peaks are the emission of the 299.95 and 304.04 nm lines, respectively. This phenomenon can be explained by the fact that Einstein transition probabilities of the 299.95 nm transition are different from those of the 304.04 nm transition as shown in Table 1-1. The Einstein coefficients A and B of the 299.95 nm transition are 0.47×10^{8} s^{-1} and 0.762×10^{20} $m^{3}J^{-1}s^{-2}$, respectively. The Einstein coefficients A and B of the 304.04 nm transition are 0.23×10^{8} s^{-1} and 0.388×10^{20} $m^{3}J^{-1}s^{-2}$, respectively. It is thought that, as the Einstein coefficient B of the

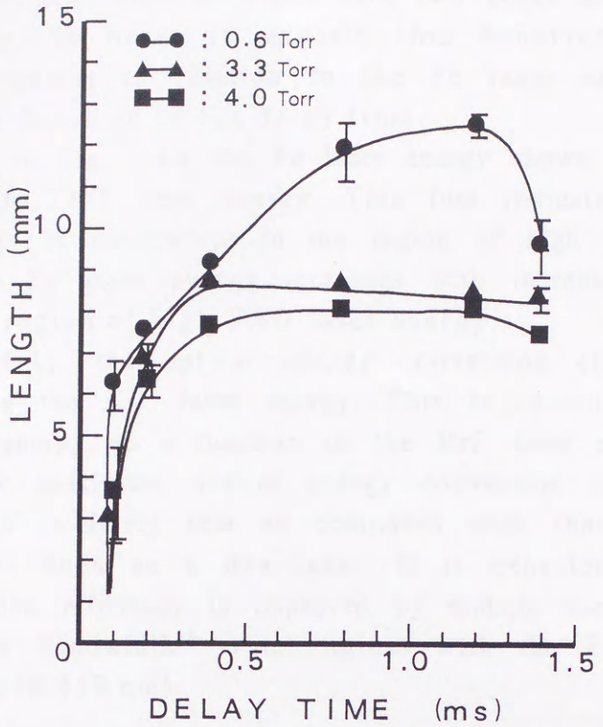

FIG. 1-12. Time variation of the horizontal length of the Fe laser medium.
(YAG laser energy:1.5 J/pulse)

299.95 nm transition is larger than that of the 304.04 nm transition, the laser oscillation of the 299.95 nm line is observed earlier than that of the 304.04 nm line.

As shown in Fig. 1-5, at 0.6 Torr the output power of the 299.95 nm line (first peak) is higher than that of the 304.04 nm line (second peak), but at 3.3 Torr it is lower than that of the 304.04 nm line. The upper state of the 299.95 and 304.04 nm lines is the same (as shown in Fig. 1-1). These above facts indicate that the population inversion density on the 299.95 nm transition decreases more than that on the 304.04 nm transition with increasing the He gas pressure, namely, that the lower state density on the 299.95 nm transition increases more than that on the 304.04 nm transition with increasing the He gas pressure. The lower state ($^5F_5$) of the 299.95 nm transition is degenerate with the lower state ($^5F_4$) of the 304.04 nm transition. Therefore, it is presumed that intramultiplet transfer of population from the $^5F_4$ state to the $^5F_5$ state occurs through collisions.[36,37]

The curve in Figs. 1-7 and 1-8 has two peaks. It is thought that this behavior is connected with temporal behaviors of the following physical quantities; (1)the density of the upper or lower laser state, (2)the length of the laser medium. The length of the laser medium as a

function of the delay time does not have two peaks as shown in Fig. 1-12. Therefore, in order to explain this behavior, the density of fundamental species in relation to the Fe laser oscillation must be measured as a function of the delay time.

As shown in Fig. 1-10, the Fe laser energy shows a saturation in the region of high YAG laser energy. This fact indicates that the optical pumping energy is insufficient in the region of high YAG laser energy. Therefore, the Fe laser energy increases with increasing the KrF laser energy in the region of high YAG laser energy.

In Fig. 1-11, the optical energy conversion efficiency decreases with increasing the KrF laser energy. This is caused by the fact that the Fe laser energy as a function of the KrF laser energy shows some saturation. The maximum optical energy conversion efficiency is 6.5×10^{-3} %, which is fairly low as compared with that of other optical pumping lasers such as a dye laser. It is expected that the optical energy conversion efficiency is improved by making use of the KrF laser with a narrow bandwidth[38] which agrees with the Fe absorption lines (248.327 and 248.419 nm).

1-3-2. Output characteristics of visible lines

Figure 1-13 shows a spectrogram showing the wavelength of the visible Fe laser lines. The reference spectra are neon lines. The measured values of the wavelength are 532.446 $\pm$0.176 and 562.408 $\pm$0.166 nm.

Figure 1-14 shows an oscillogram of the KrF laser pulse for optically pumping and the visible Fe laser pulse at the He buffer gas pressure of 3.3 Torr and the delay time of 1.0 ms. The pulse duration and width (FWHM) of the KrF laser are about 20 and 8 ns, respectively. The visible Fe laser pulse has two peaks as same as the ultraviolet Fe laser pulse as shown in the previous paragraph. The first and second peaks exist at about 10 and 15 ns after the KrF laser irradiation, respectively. The pulse duration of the visible Fe laser is about 18 ns.

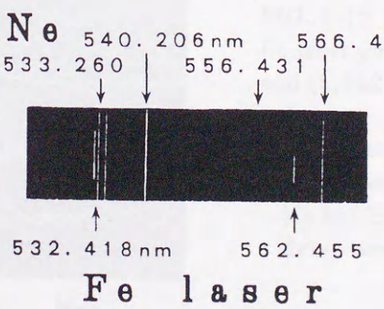

FIG. 1-13. Spectrogram showing the wavelength of the visible Fe laser lines.

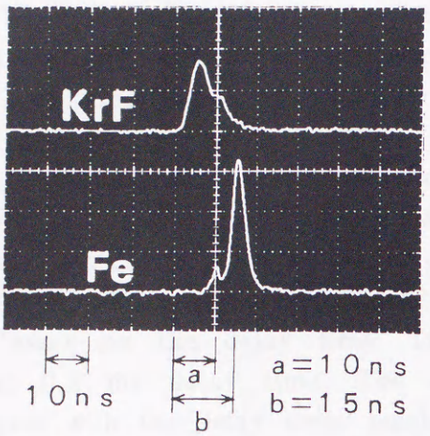

FIG. 1-14. Oscillogram of the KrF laser pulse and the visible Fe laser pulse.
(YAG laser energy:2.0 J/pulse)

Figures 1-15(a) and 1-15(b) show oscillograms of the visible Fe laser pulses of 532.42 and 562.46 nm with the KrF laser pulse, respectively. The laser oscillation of the 562.46 nm line is observed earlier than that of the 532.42 nm line. The outputs of the 562.46 and 532.42 nm lines show the peaks at about 10 and 15 ns after the KrF laser irradiation, respectively. In comparison of Figs. 1-14 and 1-15, therefore, it is confirmed that the first and second peaks are the lights of the 562.46 and 532.42 nm lines, respectively.

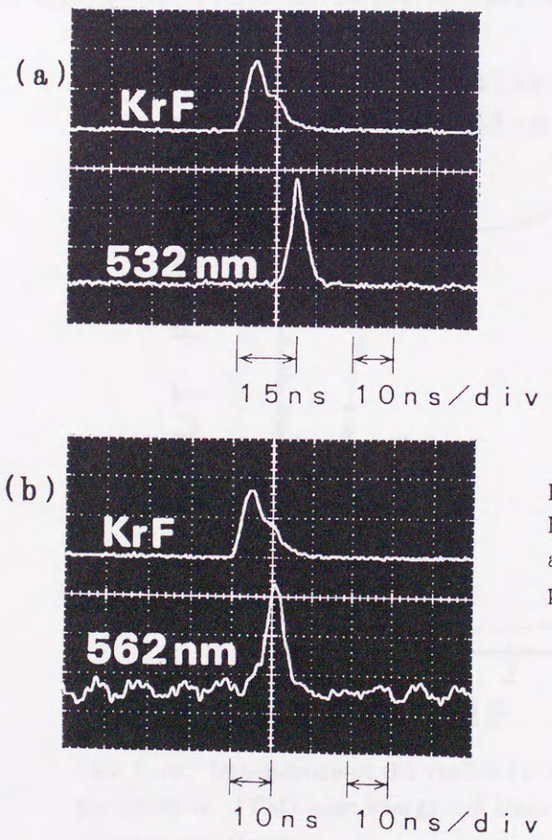

FIG. 1-15. Oscillograms of the visible Fe laser pulses of (a)532.42 nm line and (b)562.46 nm line with the KrF laser pulse.
(YAG laser energy:2.0 J/pulse,
KrF laser energy:34 mJ/pulse,
He buffer gas pressure:3.3 Torr,
delay time:1.0 ms)

Figure 1-16 shows the dependence of the output powers of the visible Fe lasers on the He buffer gas pressure. The output power of the 562.46 nm line gradually increases with increasing the He buffer gas pressure. The output power of the 532.42 nm line rapidly increases with increasing the He buffer gas pressure, reaches a maximum at 3.3 Torr and then decreases. In the examined pressure region, the output power of the 532.42 nm line larger than that of the 562.46 nm line.

Figure 1-17 shows the dependence of the output powers of the visible Fe lasers on the delay time. The visible Fe lasers are observed after about 0.2 ms delay time. The output powers of the visible Fe lasers increase with the delay time, reach a maximum at 1.2 ms and then rapidly decrease with decreasing the YAG laser power. The output power of the 532.42 nm line is larger than that of the 562.46 nm line. The maximum output powers of the 532.42 and 562.46 nm lines are about 16.8 and 1.1 W, respectively.

Figure 1-18 shows the dependence of the visible Fe laser energy on the YAG laser energy for vaporization. The visible Fe laser is observed from the YAG laser energy of about 1.0 J/pulse. The visible Fe laser energy increases with increasing the YAG laser energy, showing somewhat a saturation. When the YAG laser energy is 2.0 J/pulse, the maximum laser energy of 135.3 nJ/pulse is obtained.

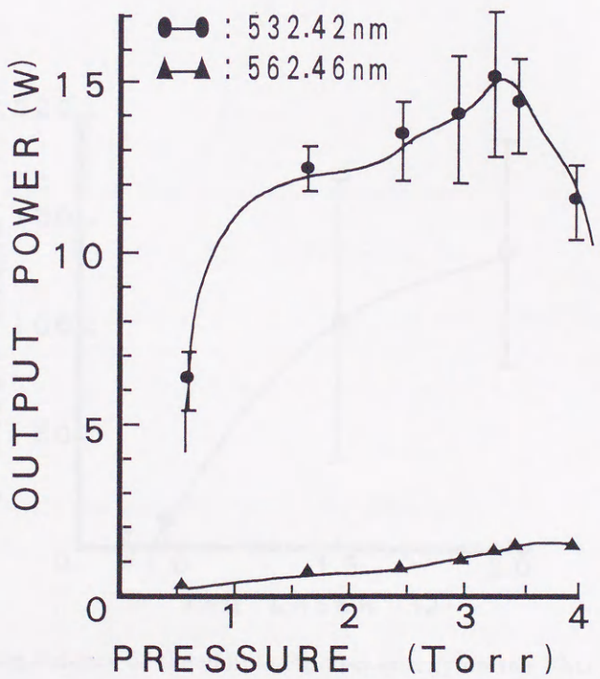

FIG. 1-16. Dependence of the visible Fe laser output power on the He buffer gas pressure. (YAG laser energy:2.0 J/pulse, KrF laser energy:34 mJ/pulse, delay time:1.0 ms)

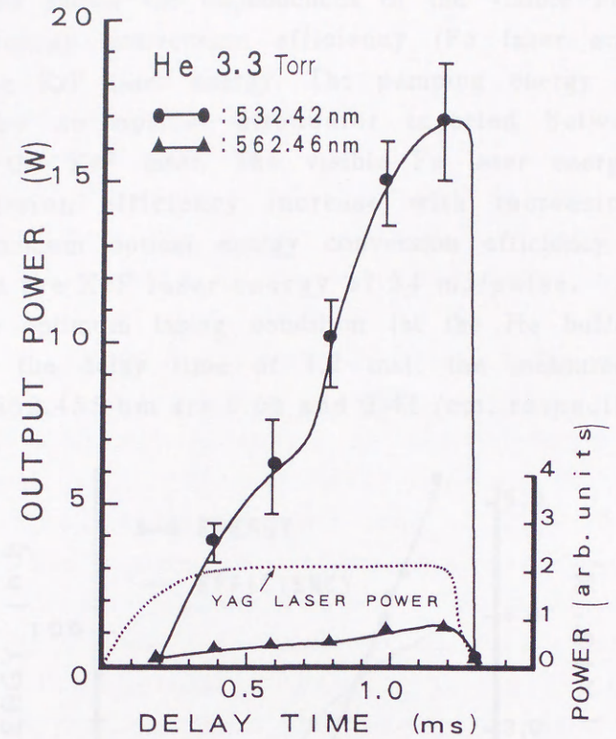

FIG. 1-17. Dependence of the visible Fe laser output power on the delay time. (YAG laser energy:2.0 J/pulse, KrF laser energy:3.4 mJ/pulse, He buffer gas pressure:3.3 Torr)

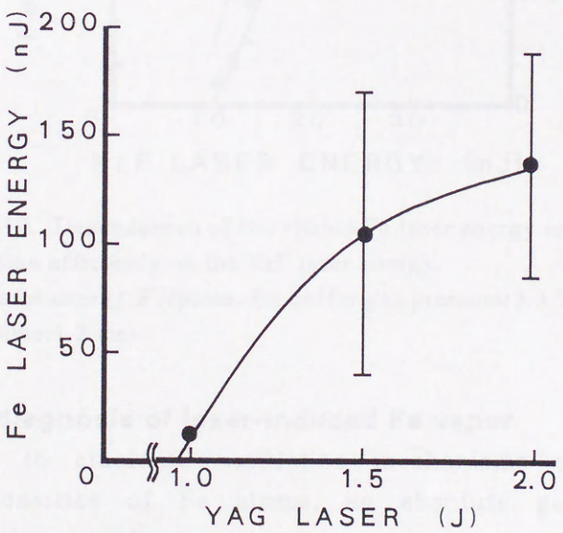

FIG. 1-18. Dependence of the visible Fe laser energy on the YAG laser energy. (KrF laser energy:34 mJ/pulse, He buffer gas pressure:3.3 Torr, delay time:1.2 ms)

Figure 1-19 shows the dependences of the visible Fe laser energy and the optical energy conversion efficiency (Fe laser energy / KrF laser energy) on the KrF laser energy. The pumping energy (KrF laser energy) is changed by an optical attenuator inserted between the Fe laser chamber and the KrF laser. The visible Fe laser energy and the optical energy conversion efficiency increase with increasing the KrF laser energy. A maximum optical energy conversion efficiency of 3.98×10^{-4} % is obtained at the KrF laser energy of 34 mJ/pulse.

Under the optimum lasing condition (at the He buffer gas pressure of 3.3 Torr and the delay time of 1.2 ms), the measured optical gains at 532.418 and 562.455 nm are 0.66 and 0.41 /cm, respectively.

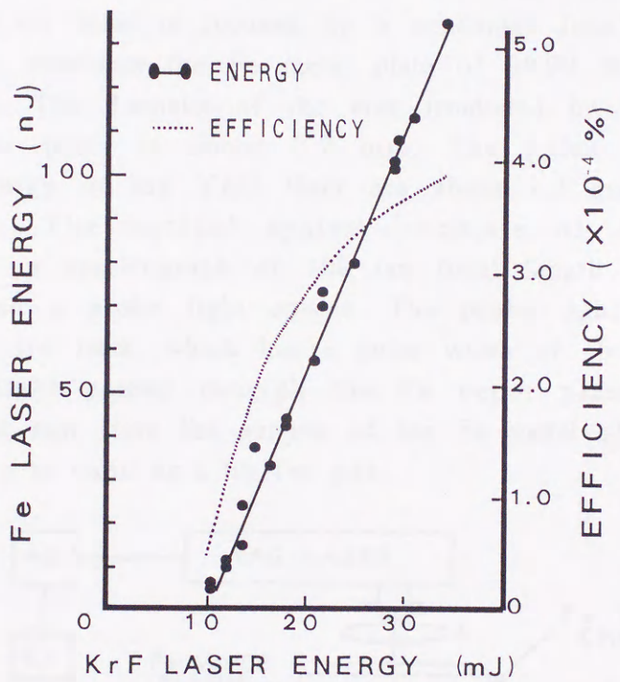

FIG. 1-19. Dependences of the visible Fe laser energy and the optical energy conversion efficiency on the KrF laser energy.
(YAG laser energy:2 J/pulse, He buffer gas pressure:3.3 Torr, delay time:1.2 ms)

1-4. Plasma diagnosis of laser-induced Fe vapor

In order to elucidate oscillation mechanisms of the Fe vapor laser, population densities of Fe atoms, an absolute gas temperature and an electron density in the vapor plasma are measured by using the hook method, the Boltzmann plot method and the Saha ionization theory, respectively.[23-27] In the measurement of the absolute gas temperature, it is experimentally confirmed that the Fe vapor plasma is in local thermodynamic equilibrium (LTE).

An absorption coefficient of the KrF laser by Fe atoms is also measured.

1-4-1. Measurement of plasma parameters

A. Measurement of population density

The population densities of Fe atoms in the vapor plasma are measured by using the hook method.[23,24] This method is an interferometric measurement of anomalous dispersion in the neighborhood of an absorption line.

Figure 1-20 shows a schematic diagram of the experimental setup, which consists of an Fe laser chamber, a pulsed Nd:YAG laser for vaporization, and an optical system for the interferometric measurement. The pulsed YAG laser is focused by a condenser lens of 100 mm focal length and it irradiates the Fe metal plate of 99.99 % purity in the Fe laser chamber. The diameter of the area irradiated by the YAG laser on the Fe metal plate is about 0.7 mm. The pulse duration and the irradiating energy of the YAG laser are about 1.3 ms and 2.0 J/pulse, respectively. The optical system consists of a Mach-Zehnder interferometer, a spectrograph of 100 cm focal length with a grating of 2400 /mm and a probe light source. The probe light source is an N_2 -laser-pumped dye laser, which has a pulse width of about 8 ns (FWHM). The probe light passes through the Fe vapor plasma at a vertical distance of 12 mm from the surface of the Fe metal plate. A He gas of 99.9 % purity is used as a buffer gas.

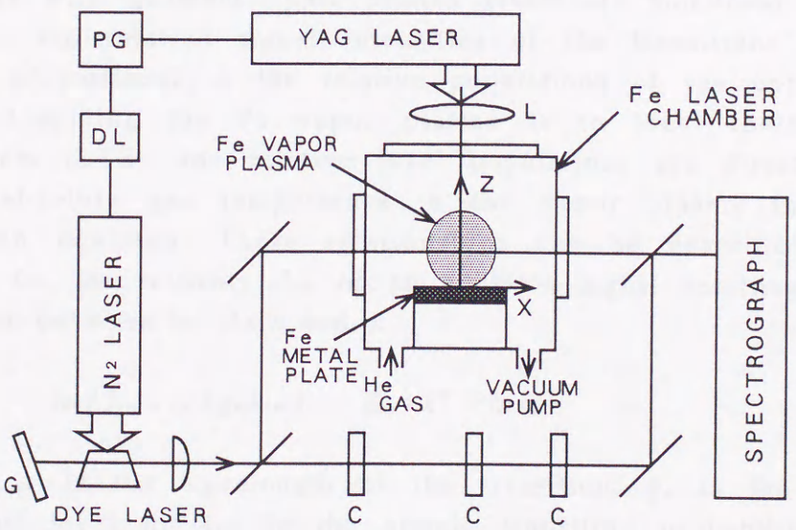

FIG. 1-20. Schematic diagram of the experimental setup for measuring the population density.
(PG:pulse generator, DC:delay circuit, L:condenser lens, G:grating, C:compensator)

TABLE 1-2. Data on the hook measurement.

Transition (Upper level —Lower level)	Spectral line (nm)	f value	Dye solution (solvent)
$3d^6 4s\ (^6D)\ 4p\ {}^5F^o_5 - 3d^6 4s^2\ {}^5D_4$	371.994	0.047	
$3d^6 4s\ (^6D)\ 4p\ {}^5F^o_2 - 3d^6 4s^2\ {}^5D_1$	374.826	0.030	BPBD-365 (toluene /ethanol)
$3d^7\ (^4F)\ 4p\ {}^5F^o_5 - 3d^7\ (^4F)\ 4s\ {}^5F_5$	373.487	0.382	
$3d^7\ (^4F)\ 4p\ {}^5D^o_3 - 3d^7\ (^4F)\ 4s\ {}^5F_4$	382.588	0.271	

The output of the spectrograph is an interference pattern, which contains "hooks" caused by the anomalous dispersion around atomic absorption lines. The densities of Fe atoms are obtained by measuring a path length of the probe light through the Fe vapor plasma and a wavelength separation between the hooks in the interference pattern.

Table 1-2 shows the transitions examined in this work, the absorption oscillator strengths (f values) for the transitions and the dye solution employed as the probe light source.[33]

B. Measurement of absolute gas temperature

The Boltzmann plot method is employed for measuring the absolute gas temperature in the Fe vapor plasma.[23-25] If a series of atomic transitions with different upper excited levels are monitored by atomic emission, the relative signal intensities of the transitions should be directly proportional to the relative populations of the upper excited levels. Assuming the Fe vapor plasma is in local thermodynamic equilibrium (LTE), the relative level populations are directly related to the absolute gas temperature in the vapor plasma through the Boltzmann equation. These relationships can be described with an equation for the intensity I_{nm} of an emission signal resulting from the transition between levels n and m,

$$ln\,(I_{nm}\lambda_{nm} / g_n A_{nm}) = -E_{ex} / kT + ln\,C, \quad (1)$$

where λ_{nm} is the wavelength of the transition, g_n is the statistical weight of level n, A_{nm} is the atomic transition probability for the transition, E_{ex} is the excitation energy of level n, k is the Boltzmann constant, C is the constant value, and T represents the absolute gas temperature of the vapor plasma.[23-25] A plot of $ln(I_{nm}\lambda_{nm} / g_n A_{nm})$ versus E_{ex} for a series of atomic transitions results in a straight line

with a slope of $-1/kT$, allowing for the determination of T. The intensities of Fe I lines which are emitted from the center of the vapor are measured by using a photomultiplier through the spectrometer with concealing from the light of the irradiating point of the YAG laser. The Boltzmann plot method requires accurate gA values for transitions, preferably with a large separation in energy. Table 1-3 summarizes the physical data for the Fe I lines used in this work.[28-30]

TABLE 1-3. Spectroscopic data for Fe I lines used in the measurement of the absolute gas temperature.
(λ :wavelength, E_{ex} :excitation energy of the upper level, g:statistical weight of the upper level, A:Einstein transition probability)

λ (nm)	Eex (cm^{-1})	gA ($10^8 s^{-1}$)
401.153	53722	17.0
402.187	47107	5.4
406.359	37163	9.9

C. Measurement of electron density

The electron density in the laser-induced Fe vapor plasma is measured by using the Saha ionization theory.[26,27] The electron density in the Fe vapor plasma is obtained by measuring the intensity ratio of ion to neutral atom lines. The intensities of Fe I and Fe II lines which are emitted from the Fe vapor plasma are measured. The electron density (Ne) is given by

$$Ne = 4.83\times10^{15}T^{3/2}(I_a/I_i)(g_iA_i\lambda_a/g_aA_a\lambda_i) \times exp((E_a-E_i-V)/kT), \quad (2)$$

where T is the absolute temperature of the vapor plasma, I_a and I_i are the intensities of Fe I and Fe II lines, g_a and g_i are the statistical weights of the upper levels of Fe I and Fe II lines, A_i and A_a are the Einstein transition probabilities of Fe I and Fe II lines, λ_a and λ_i are the wavelengths of Fe I and Fe II lines, E_a and E_i are the excitation energies of the upper levels of Fe I and Fe II lines, V is the ionization energy of Fe atom (about 63480 cm^{-1}), and k is the Boltzmann constant.

Table 1-4 lists the physical data for Fe I and Fe II lines used in the measurements of the electron density.[33,39]

TABLE 1-4. Data on the measurement of the electron density.
(λ :wavelength, E_{ex} :excitation energy of the upper level of the transition, g_a and g_i :statistical weights of the upper levels of the atomic and ionic transitions, A_a and A_i :Einstein transition probabilities of the atomic and ionic transitions, λ_a and λ_i :wavelengths of the atomic and ionic transitions)

	λ (nm)	Eex (cm^{-1})	($g_iA_i\lambda_a/g_aA_a\lambda_i$)
Fe I	252.285	39626	3.135
Fe II	258.588	38660	

D. Measurement of absorption coefficient

An absorption of the KrF laser by Fe atoms is measured by making a comparison with the input and output KrF laser intensities at 248.327 and 248.419 nm. The absorption is defined as the ratio of the output KrF laser intensity after passing through the vapor plasma to the input KrF laser intensity. The KrF laser radiation at about 248 nm is recorded on a spectrograph of 100 cm focal length with a grating of 1200 /mm in the third order, which is examined by means of a densitometer.

The absorption coefficient μ is given by

$$I_{out} = I_{in}\exp(-\mu L), \tag{3}$$

where I_{out} is the output KrF laser intensity, I_{in} is the input KrF laser intensity, and L is the pass length of the KrF laser through the Fe vapor plasma.[40]

1-4-2. Characteristics of laser-induced Fe vapor plasma

A. population density

The time variations of the density of Fe atoms in the ground-state [$3d^64s^2\ ^5D_4$] at 0.6 and 3.3 Torr are shown in Figs. 1-21(a) and 1-21(b), respectively. A curve in the figure is to guide the reader's eye. In Fig. 1-21(a), the density of Fe atoms in the ground-state at 0.6 Torr increases with time, reaches a maximum at about 0.6 ms and then decreases monotonously. The curve has a hollow at about 0.2 ms. The maximum value of the density at about 0.6 ms is about 8.0×10^{14} cm^{-3}.

In Fig. 1-21(b), the density of Fe atoms in the ground-state at 3.3 Torr increases with time, takes two peaks at about 0.4 and 1.2 ms, and then decreases. The curve has a hollow at about 0.7 ms. The maximum value of the density at about 1.2 ms is about 1.0×10^{15} cm^{-3}. The density in the ground-state at 3.3 Torr is slightly larger than that at 0.6 Torr.

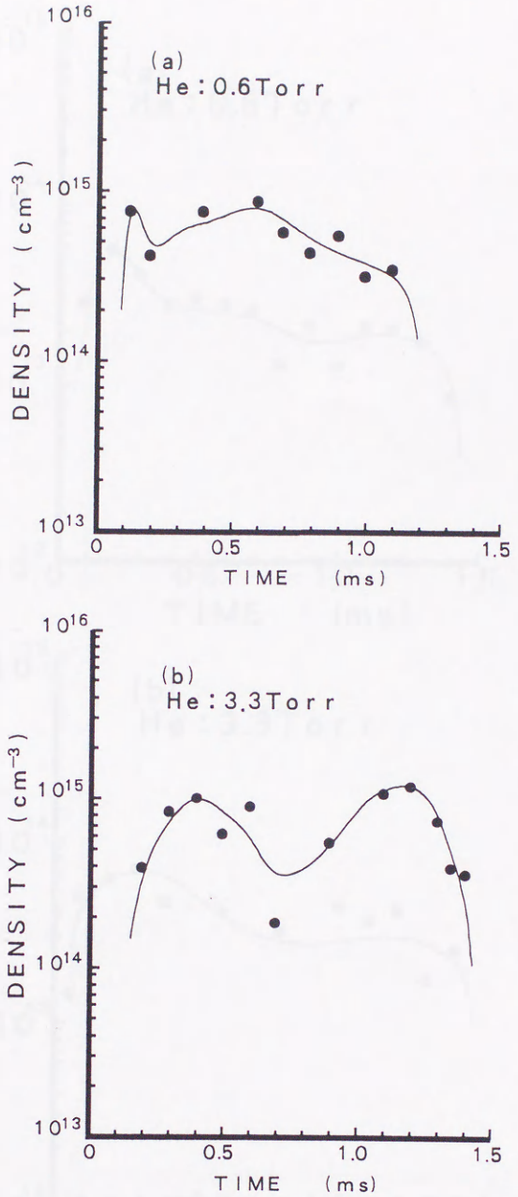

FIG. 1-21.
Time variation of the density of Fe atoms in the ground-state [$3d^6\,4s^2\ ^5D_4$]:
(a)at 0.6 Torr, (b)at 3.3 Torr.

Figures 1-22(a) and 1-22(b) show the time variations of the density of Fe atoms in the metastable state [$3d^7(^4F)4s\ ^5F_5$] at 0.6 and 3.3 Torr, respectively. The density of Fe atoms in the $^5F_5$ state increases rapidly with time, and then monotonously decreases. The average values of the density at 0.6 and 3.3 Torr are about 2.5×10^{13} and 3.7×10^{13} cm^{-3}, respectively. The density of Fe atoms in the $^5F_5$ state is an order of magnitude smaller than that in the ground-state.

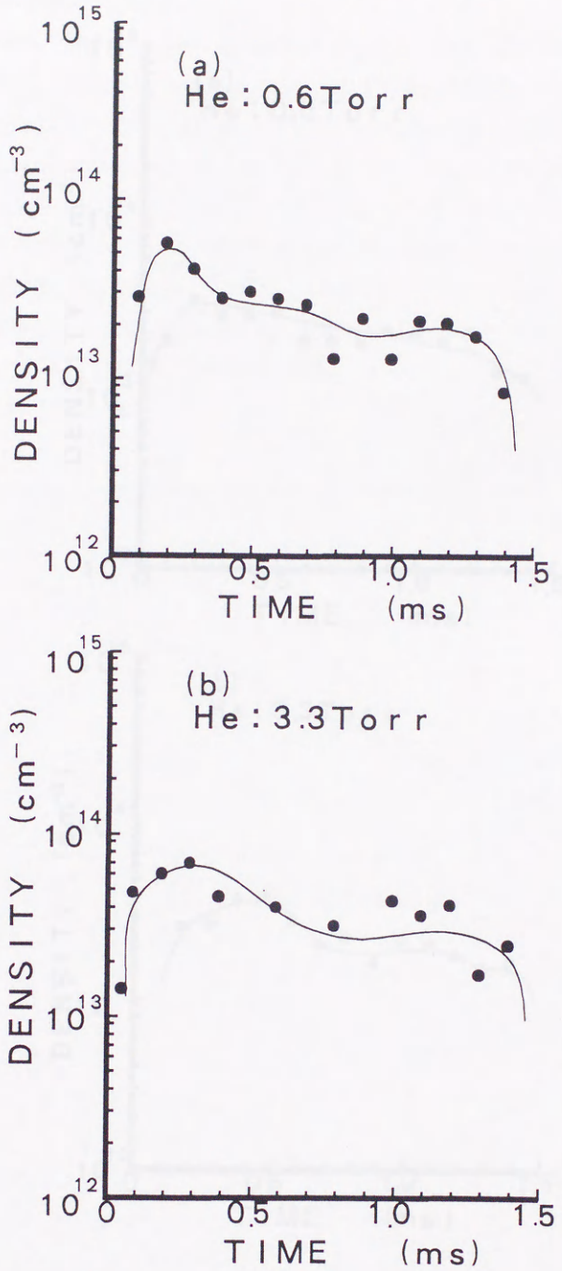

FIG. 1-22. Time variation of the density of Fe atoms in the metastable state $[3d^7(^4F)4s\ ^5F_5]$; (a)at 0.6 Torr, (b)at 3.3 Torr.

Figures 1-23(a) and 1-23(b) show the time variations of the density of Fe atoms in the metastable state $[3d^7(^4F)4s\ ^5F_4]$ at 0.6 and 3.3 Torr, respectively. The time variation of the density of Fe atoms in the $^5F_4$ state resembles that in the $^5F_5$ state, because the $^5F_4$ state is degenerate with the $^5F_5$ state. The average values of the density at 0.6 and 3.3 Torr are about 2.5×10^{13} and 2.8×10^{13} cm^{-3}, respectively.

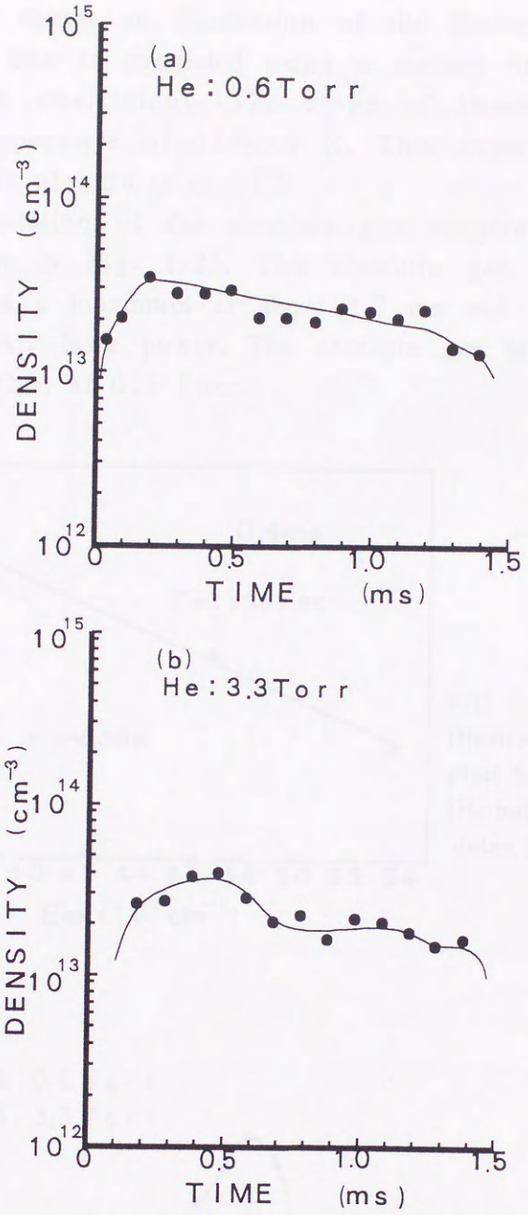

FIG. 1-23. Time variations of the density of Fe atoms in the metastable state [$3d^7$ (^{4}F)$4s$ $^5F_4$]; (a)at 0.6 Torr, (b)at 3.3 Torr.

In comparison of Figs. 1-22 and 1-23, at 0.6 Torr the population density of Fe atoms in the $^5F_5$ state is almost equal to that in the $^5F_4$ state, whereas at 3.3 Torr the population density in the $^5F_5$ state is larger than that in the $^5F_4$ state. This can be explained by the fact that intramultiplet transfer of population from the $^5F_4$ state to the $^5F_5$ state occurs through collisions.[36,37]

B. Absolute gas temperature

Figure 1-24 shows an illustration of the Boltzmann plots for Fe I lines. The solid line is computed using a method of least squares, and r is a correlation coefficient. The slope of these plots provides the absolute gas temperature of 11387.9 K. This experimental results shows that the Fe vapor plasma is in LTE.

The time variation of the absolute gas temperature in the Fe vapor plasma is shown in Fig. 1-25. The absolute gas temperature increases with time, reaches a maximum at about 1.2 ms and rapidly decreases with decreasing the YAG laser power. The absolute gas temperature at 3.3 Torr is higher than that at 0.6 Torr.

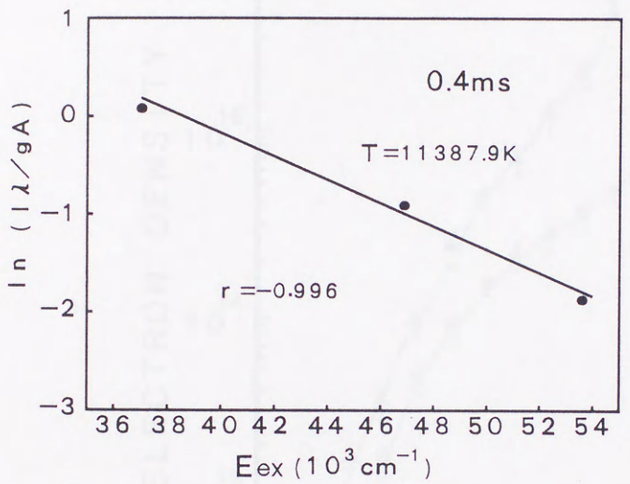

FIG. 1-24.
Illustration of the Boltzmann plots for Fe I lines.
(He buffer gas pressure:3.3 Torr, delay time:0.4 ms)

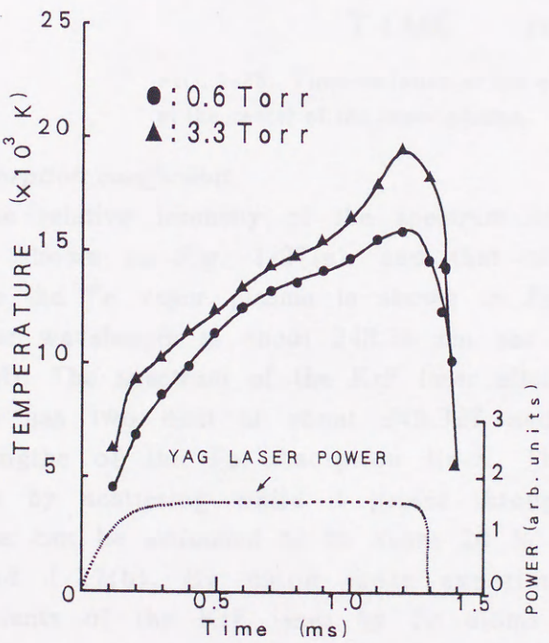

FIG. 1-25.
Time variation of the gas temperature at the center of the vapor plasma.

C. Electron density

Figure 1-26 shows the time variation of the electron density in the Fe vapor plasma. The electron density increases with time, reaches a maximum at about 1.2 ms, and rapidly decreases. The electron density at 3.3 Torr is larger than that at 0.6 Torr. The maximum value of 1.3×10^{15} cm^{-3} is obtained at 3.3 Torr and 1.2 ms. In comparison of Figs. 1-25 and 1-26, the time variation of the electron density resembles that of the absolute gas temperature.

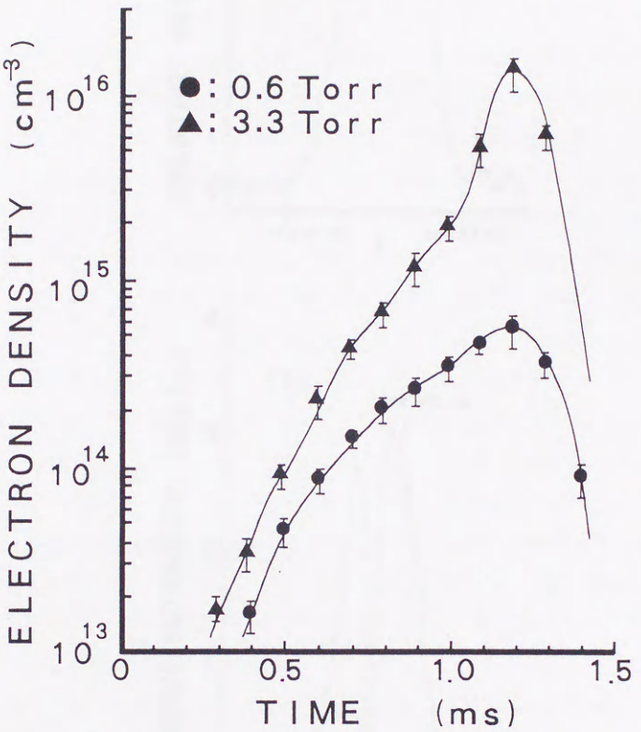

FIG. 1-26. Time variation of the electron density at the center of the vapor plasma.

D. Absorption coefficient

The relative intensity of the spectrum of the KrF laser at about 248 nm is shown in Fig. 1-27(a), and that of the KrF laser after passing through the Fe vapor plasma is shown in Fig. 1-27(b). The KrF laser has a center wavelength at about 248.34 nm and a linewidth of about 0.17 nm (FWHM). The spectrum of the KrF laser after passing through the Fe vapor plasma has two dent at about 248.327 and 248.419 nm, which are the wavelengths of the Fe absorption lines. The intensity of the KrF laser is lost by scattering while it passes through the Fe vapor plasma, and the loss can be estimated to be about 20 % from comparison of Figs. 1-27 (a) and 1-27(b). By using these experimental results, the absorption coefficients of the KrF laser by Fe atoms are obtained. The absorption coefficients at 248.327 and 248.419 nm are shown in Table 1-5.

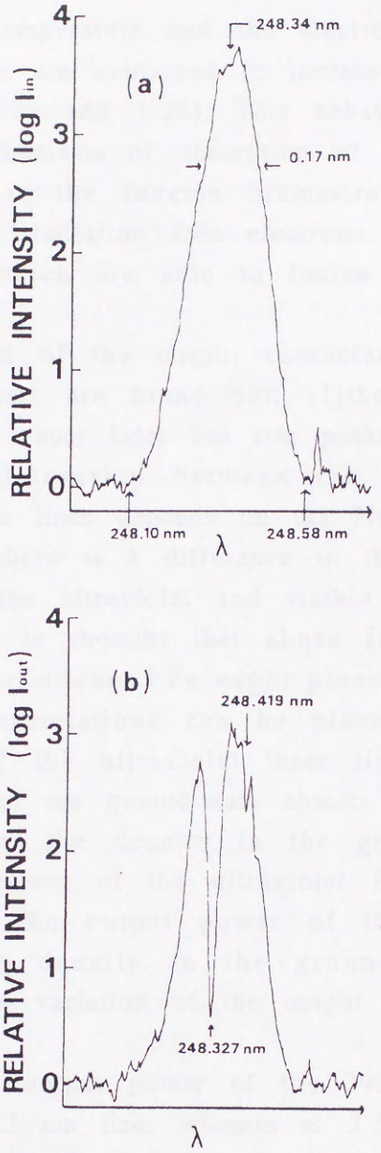

FIG. 1-27. Densitometer traces of (a)the KrF laser spectrum and (b)the after passing through the Fe vapor plasma. (at 3.3 Torr and at 1.0 ms)

TABLE 1-5. Absorption coefficients at 248.327 and 248.419 nm.
(He buffer gas pressure:3.3 Torr, delay time:1.0 ms)

λ (nm)	μ (/cm)
248.327	1.374[a], 2.221[b]
248.419	0.245[a], 0.401[b]

a: He pressure of 0.6 Torr and delay time of 0.4 ms.
b: He pressure of 3.3 Torr and delay time of 1.0 or 1.2 ms.

1-5. Discussion

The absolute gas temperature and the electron density at the center of the Fe vapor plasma are continued to increase during the YAG laser irradiation (see Figs. 1-25 and 1-26). This behavior is explained by the fact that the main mechanisms of absorption of the YAG laser radiation in the vapor plasma is the inverse bremsstrahlung process, that is, during the YAG laser irradiation free electrons obtain energy from the laser radiation field, which are able to ionize a neutral atom in the vapor plasma.[41,42]

In the measurement of the output characteristics of the Fe vapor laser, the following facts are found out; (1)the time variation of the output power of the Fe vapor laser has two peaks as shown in Fig. 1-6, (2)the quantitative relationship between the output powers of the 299.951 and 304.043 nm lines depends on the He buffer gas pressure as shown in Fig. 1-6, (3)there is a difference in the time variation of the output power between the ultraviolet and visible Fe lasers as shown in Figs. 1-6 and 1-17. It is thought that above facts are connected with the dynamics of the laser-induced Fe vapor plasma.

The following interpretations can be placed on the above facts. (1)The upper states of the ultraviolet laser lines are formed by the process that Fe atoms in the ground-state absorb the KrF laser as shows in Fig. 1-1. Therefore, the density in the ground-state significantly influences the output power of the ultraviolet Fe laser. As the result, the time variation of the output power of the ultraviolet Fe laser resembles that of the density in the ground-state, so it can be considered that the time variation of the output power has hollows (see Figs. 1-21 and 1-6).

(2)At 0.6 Torr the output power of the 299.951 nm line is larger than that of the 304.043 nm line, whereas at 3.3 Torr the output power of the 299.951 nm line is smaller than that of the 304.043 nm line (see Fig. 1-6). The upper state of the 299.951 and 304.043 nm lines is the same state [$3d^6 4s(^4D)4p\ ^5F^o_5$]. At 0.6 Torr the density of Fe atoms in the metastable state [$3d^7(^4F)4s\ ^5F_5$] is slightly smaller than that in the metastable state [$3d^7(^4F)4s\ ^5F_4$], whereas at 3.3 Torr the density in the $^5F_5$ state is larger than that in the $^5F_4$ state (see Figs. 1-22 and 1-23). Therefore, it is thought that the quantitative relationship between the output powers of the 299.951 and 304.043 nm lines depend on that between the densities of Fe atoms in each lower states.

(3)The time variation of the output power of the visible Fe laser is different from that of the ultraviolet Fe lasers. It is thought that the above fact is caused by the different oscillation mechanisms between the ultraviolet and visible Fe lasers. The upper states of the ultraviolet

laser lines are formed by the process that Fe atoms in the ground-state absorb the KrF laser. On the other hand, the upper state of the visible laser line is higher than the state directly pumped by the KrF laser as shown in Fig. 1-1. An energy difference between these states is about 4400 cm^{-1}, which is equivalent to the temperature of about 6300 K or to the electronic energy of about 0.55 eV. The time variation of the output power of the visible Fe laser resembles those of the temperature or the electron density (see Figs. 1-17, 1-25 and 1-26). On the basis of above facts, it is thought that the upper state of the visible laser line is formed by the collision between Fe atoms in the excited states and electrons having energy higher than 0.55 eV.

Based on above interpretations, according to the energy level diagram in Fig. 1-1, the process sequence for the formations of the laser upper and lower states is represents by a set of rate equations, which is graphically depicted in Fig. 1-28.

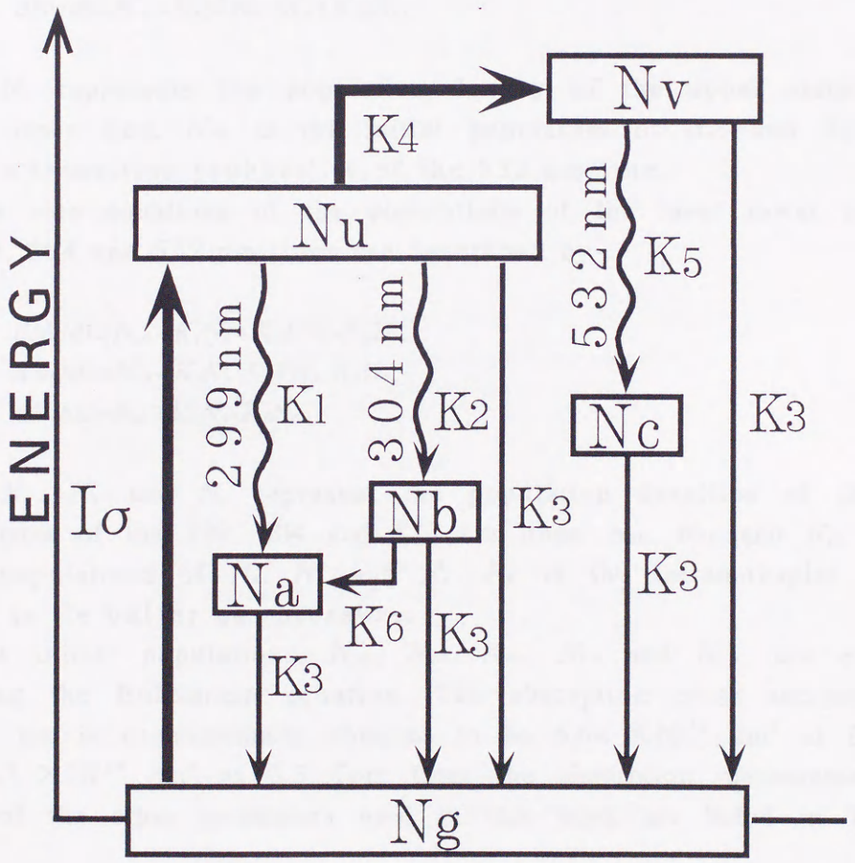

FIG. 1-28. Illustration of a process sequence for the formations of the las erupper and lower states.
(Ng:the ground-state, Nu:upper state of the ultraviolet laser lines, Nv:upper state of the visible laser line, Na:lower state of the 299.951 nm line, Nb: lower state of the 304.043 nm line, Nc:lower state of the 532.418 nm line)

The rate equation of the population of the laser upper state of the 299 and 304 nm lines is described by

$$dN_u/dt=N_{u0}+I\sigma(N_g-N_u)-(K_1+K_2+K_3+K_4N_e)N_u, \quad (a)$$

where N_u and N_g represent the population density of the upper state of the ultraviolet laser lines and the ground-state, N_{u0} is the initial population of N_u, N_e is the electron density, I is the KrF laser intensity, σ is the absorption cross section of the KrF laser by an Fe atom, K_1 and K_2 are the Einstein transition probabilities of the 299 and 304 nm lines, K_3 is the relaxation rate, K_4 is the collisional excitation rate.

The rate equation of the population of the laser upper state of the 532 nm line is described by

$$dN_v/dt=N_{v0}+K_4N_eN_u-(K_3+K_5)N_v, \quad (b)$$

where N_v represents the population density of the upper state of the visible laser line, N_{v0} is the initial population of N_v, and K_5 is the Einstein transition probability of the 532 nm line.

The rate equations of the populations of the laser lower states of the 299, 304 and 532 nm lines are described by

$$dN_a/dt=N_{a0}+K_1N_u+K_6PN_b-K_3N_a, \quad (c)$$
$$dN_b/dt=N_{b0}+K_2N_u-K_6PN_b-K_3N_b, \quad (d)$$
$$dN_c/dt=N_{c0}+K_5N_v-K_3N_c, \quad (e)$$

where N_a, N_b and N_c represent the population densities of the laser lower states of the 299, 304 and 532 nm lines, N_{a0}, N_{b0} and N_{c0} are the initial populations of N_a, N_b and N_c, K_6 is the intramultiplet transfer rate, P is He buffer gas pressure.

The initial populations, N_{u0}, N_{v0}, N_{a0}, N_{b0} and N_{c0}, are estimated by using the Boltzmann equation. The absorption cross section σ at 248.327 nm is experimentally obtained to be 6.64×10^{-16} cm^2 at 0.6 Torr and 3.17×10^{-15} cm^2 at 3.3 Torr from the absorption measurement. The values of the other parameters used in this work are listed in Table 1-6.

The expression for the optical gain is given by

$$\alpha=(ln2/\pi)^{1/2}(g_jA_{ji}/4\pi)(N_j/g_j-N_i/g_i)(\lambda^2/\Delta\nu), \quad (4)$$

where λ is the center wavelength of the transition and $\Delta\nu$ is the

TABLE 1-6. The values used in the calculation of a set of rate equations.

I	4.2×10^{23}	photon·s^{-1}·cm^{-2}
K_1	4.7×10^{7}	s^{-1}
K_2	2.3×10^{7}	s^{-1}
K_3	1.0×10^{8}	s^{-1}
K_4	1.4×10^{-7}	$cm^3\cdot s^{-1}$
K_5	7.0×10^{7}	s^{-1}
K_6	6.5×10^{7}	$s^{-1}\cdot Torr^{-1}$

Doppler width, N_i and N_j are the population in laser lower and upper state, and g_i and g_j are the statistical weight of laser lower and upper state.[40] The Doppler widths of the laser lines are estimated from the measurement of the absolute gas temperature.

The calculated optical gains by using a set of rate equations are listed in Table 1-7. The measured optical gains are summarized in Table 1-8. In comparison of Tables 1-7 and 1-8, the calculated optical gains agree well with the measured optical gains. This agreement proves the validity of the hypothesis on the process sequence for the formations of the laser upper and lower states (see Fig. 1-28).

TABLE 1-7. The calculated optical gains of Fe vapor lasers.

λ (nm)	Optical gain (/cm)	
299.951	0.72[a]	1.62[b]
304.043	0.60[a]	1.86[b]
532.418	---	0.70[c]

a:He pressure of 0.6 Torr and delay time of 0.4 ms.
b:He pressure of 3.3 Torr and delay time of 1.0 ms.
c:He pressure of 3.3 Torr and delay time of 1.2 ms.

TABLE 1-8. The measured optical gains of Fe vapor lasers.

λ (nm)	Optical gain (/cm)	
299.951	0.63[a]	1.53[b]
304.043	0.49[a]	1.77[b]
532.418	---	0.66[c]

a:He pressure of 0.6 Torr and delay time of 0.4 ms.
b:He pressure of 3.3 Torr and delay time of 1.0 ms.
c:He pressure of 3.3 Torr and delay time of 1.2 ms.

At 0.6 Torr, the calculated optical gain at 299.951 nm line is larger than that at 304.043 nm line. On the other hand, at 3.3 Torr, the calculated optical gain at 299.951 nm line is smaller than that at 304.043 nm line. This calculation is taken into consideration of intramultiplet transfer of population from the laser lower state of the 304.043 nm line to that of the 299.951 nm line. If the optical gain is calculated without intramultiplet transfer, the calculated optical gain at the 304.043 nm line at 3.3 Torr is smaller than that at the 299.951 nm line. Therefore, this result indicates that the optical gain or the output power of the Fe vapor laser is dominated by not only the transition probability of the laser line but also the population of the laser lower state.

CHAPTER 2

Laser action of optically pumped Ta vapor

2-1. Ta vapor laser

A laser oscillation of Ta I atom has been first obtained by optically pumped Ta (melting-point of 3263 K) vapor. Ta vapor is produced by irradiating a Ta metal plate with a pulsed Nd:YAG laser irradiation (2 J/pulse), and the Ta atoms are optically pumped by a KrF excimer laser (10 mJ/pulse) at about 248 nm. It is observed that a Ta vapor laser pulse has a duration of 7 ns, half width of 3 ns and peak output power of 48 W.

Figure 2-1 shows energy levels pertinent to the optically pumped Ta vapor laser.[31-33] The ground-state is $5d^36s^2\ {}^4F_{3/2}$ and the wavelength of the absorption line is 248.495 nm. The Doppler half-width of this line at the melting-point is calculated to be 7.5×10^{-4} nm. The laser upper levels are $5d^4({}^5D)6p\ {}^6F^\circ_{3/2}$ and $5d^4({}^5D)6p\ {}^6F^\circ_{1/2}$.

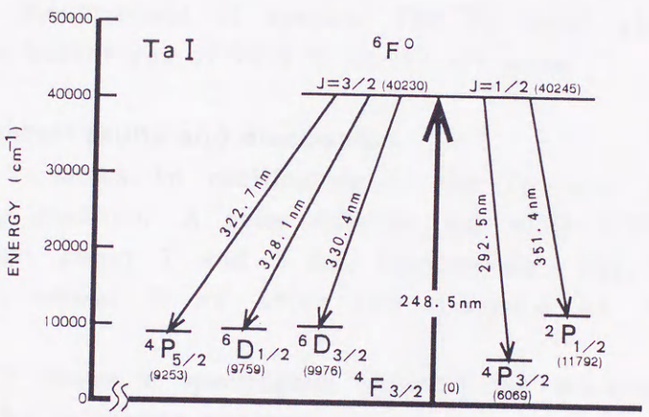

FIG. 2-1. Energy levels of Ta I pertinent to the Ta vapor laser.

2-2. Experimental methods

The experimental arrangement used in this work is essentially the same as that of the Fe vapor laser. The Ta laser system consists of a pulsed Nd:YAG laser for producing the Ta vapor, the KrF laser for optically pumping Ta vapor, a Ta laser chamber and an optical cavity. The reflectivity of the laser mirror is about 88 % at 290 ~390 nm, and that of the laser output mirror is about 71 % at 293 nm, 87 % at 320 ~ 330 nm and 91 % at 340 ~370 nm, respectively. The pulse duration and width (FWHM) of the KrF laser are 15 and 5 ns, respectively. The rise time of the KrF laser pulse is about 4 ns which is shorter than the lifetime (about 14 ns) of the Ta resonance transition.[33] The KrF laser irradiates the vapor through a rectangular slit (about 13 mm in width × 10 mm in high). The irradiating energy of the KrF laser in the laser chamber after passing through the quartz window is 10±1.0 mJ/pulse.

In order to measure the time variation of the output power of the Ta vapor laser, the KrF laser is operated by a trigger pulse with a predetermined delay time. The delay time of the trigger pulse supplied to the KrF laser after the starting of the YAG laser irradiation is determined by observing the signals of the KrF and YAG laser lights displayed on an oscilloscope.

In order to measure the dimension of the vapor, the KrF laser irradiates the vapor with a certain delay time and an image of the fluorescence is photographed through an optical band-pass filter (270 ~ 420 nm). The maximum horizontal length of the laser medium is measured from the profile of fluorescence obtained on the photograph.

An optical gain of the Ta vapor laser is measured by using the same method as the case of the Fe vapor laser.[35]

A spectrometer of 100 cm focal length with a grating of 1200 /mm is used for the measurement of spectra. The Ta metal plate of 99.95 % purity and He buffer gas of 99.9 % purity are used.

2-3. Experimental results and discussion

Figure 2-2 shows an oscillogram of the Ta laser pulse under the optimum lasing condition. A pulse duration and width (FWHM) of the Ta vapor laser are about 7 and 3 ns, respectively. The Ta vapor laser oscillates at about 5 ns after the starting of the KrF laser irradiation.

Figure 2-3 shows a spectrogram showing the wavelength of the Ta laser lines. The reference spectra are mercury lines.

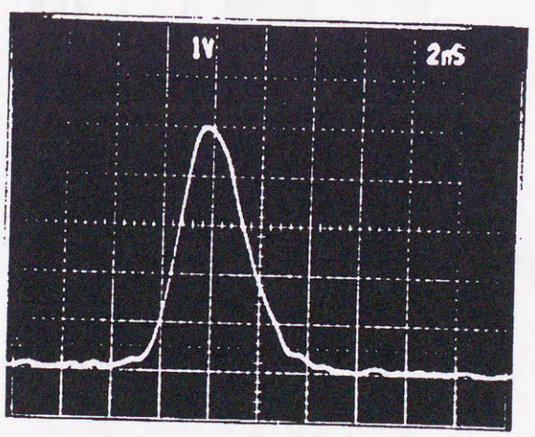

FIG. 2-2. Oscillogram of the Ta laser pulse under the optimum lasing condition. (He gas pressure:2.5 Torr, delay time:1.3 ms)

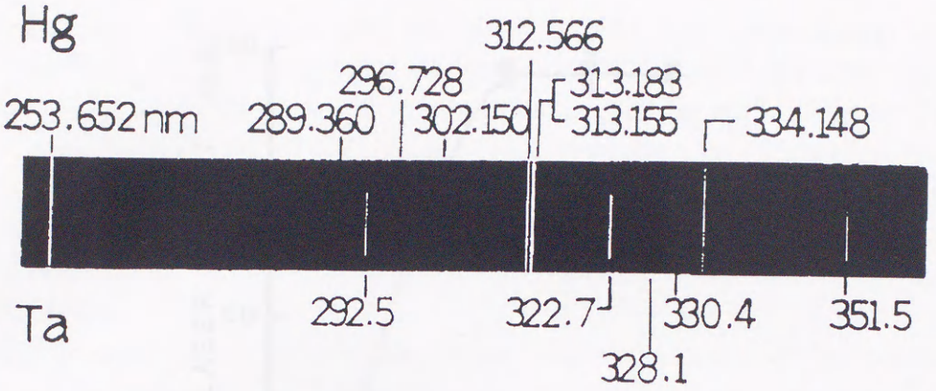

FIG. 2-3. Spectrogram showing the wavelength of the Ta laser lines.

Figure 2-4 shows the dependence of the Ta laser output energy on the delay time. The Ta laser oscillation is observed from the delay time of 0.3 ms. The output energy rapidly increases with time, has two peaks at 0.6 and 1.3 ms, and then decreases with decreasing the YAG laser power. The maximum output energy of 144 nJ/pulse is obtained at 2.5 Torr and 1.3 ms.

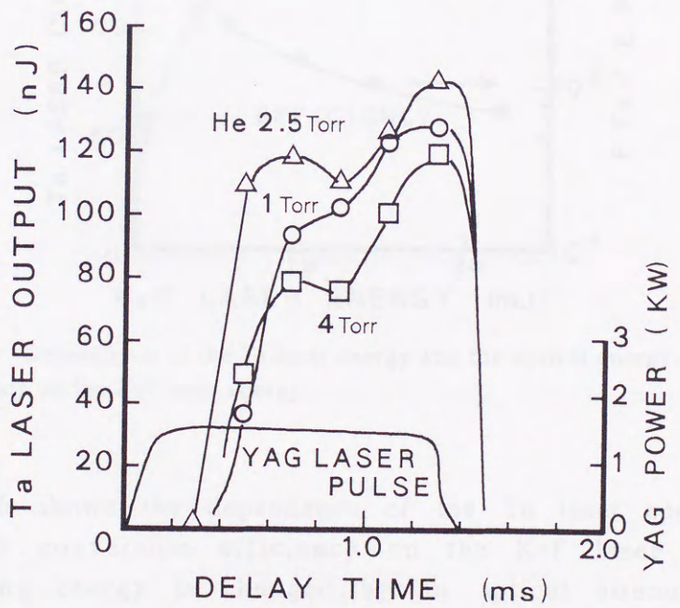

FIG. 2-4. Dependence of the Ta laser output energy on the delay time.

Figure 2-5 shows the dependence of the Ta laser energy on the YAG laser energy. The Ta laser oscillation is observed from about 1.0 J. The Ta laser output energy increases linearly with increasing the YAG laser energy and shows a saturation at the energy more than about 2.0 J.

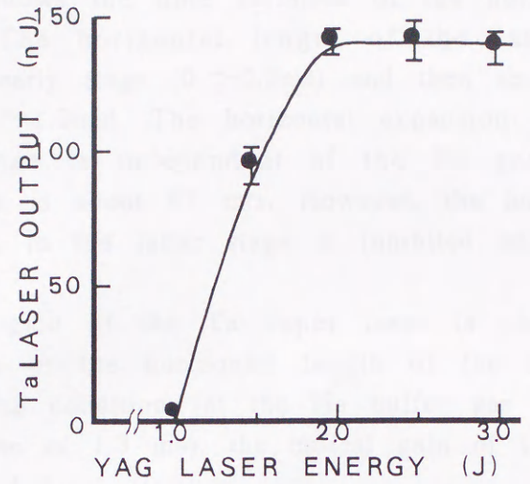

FIG. 2-5. Dependence of the Ta laser energy on the YAG laser energy.

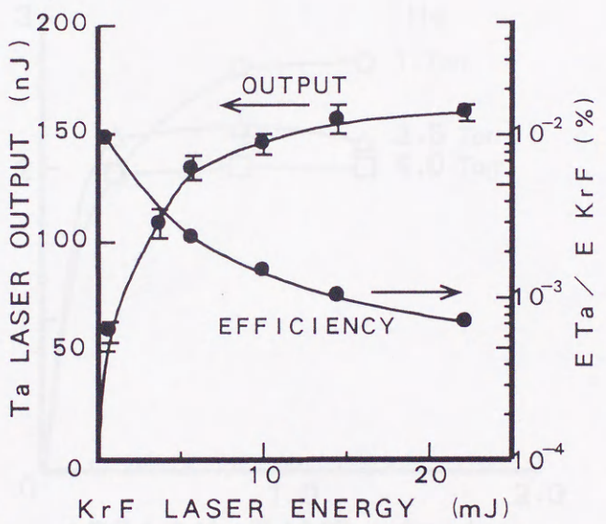

FIG. 2-6. Dependence of the Ta laser energy and the optical energy conversio nefficiency on the KrF laser energy.

Figure 2-6 shows the dependence of the Ta laser energy and the optical energy conversion efficiency on the KrF laser energy. The optical pumping energy is changed by an optical attenuator inserted between the Ta laser chamber and the KrF laser. The Ta laser output energy increases with increasing the optical pumping energy. The maximum output energy of 160 nJ/pulse is obtained at an optical pumping energy of 22.4 mJ/pulse. Contrary to the variation of the output energy, the optical energy conversion efficiency decreases with increasing the optical pumping energy, and the maximum value of 0.01 % is obtained at the optical pumping energy of 0.6 mJ/pulse.

Figure 2-7 shows the time variation of the horizontal length of the laser medium. The horizontal length of the laser medium rapidly increases in the early stage (0 ~0.3ms) and then shows a plateau in the latter stage (0.3 ~1.3ms). The horizontal expansion of the laser medium in the early stage is independent of the He gas pressure, and the expansion velocity is about 67 m/s. However, the horizontal expansion of the laser medium in the latter stage is inhibited with increasing the He gas pressure.

The optical gain of the Ta vapor laser is obtained by using the experimental data of the horizontal length of the laser medium. Under the optimum lasing condition (at the He buffer gas pressure of 2.5 Torr and the delay time of 1.3 ms), the optical gain of the Ta vapor laser is listed in Table 2-1.

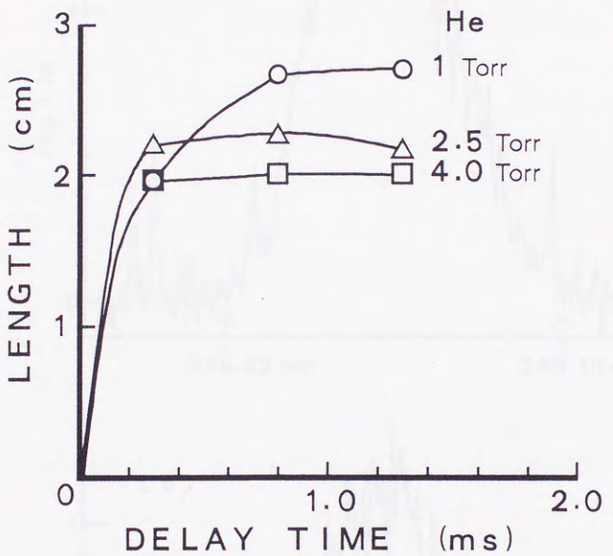

FIG. 2-7. Dependence of the horizontal length of the laser medium on the delay time.

TABLE 2-1. Wavelength and gain of the Ta vapor laser.

Wavelength (nm)	Optical Gain (/cm)
292.519	0.35
322.732	0.24
328.087	0.09
330.438	0.09
351.361	0.20

The relative intensity (I_{in}) of the spectral line at 248 nm of the KrF laser used in this work is shown in Fig. 2-8(a), and the relative intensity (I_{out}) of the KrF laser after passing through the Ta vapor plasma at the delay time of 1.3 ms is shown in Fig. 2-8(b). The center wavelength and the linewidth (FWHM) of the KrF laser are 248.37 and 0.18 nm, respectively.

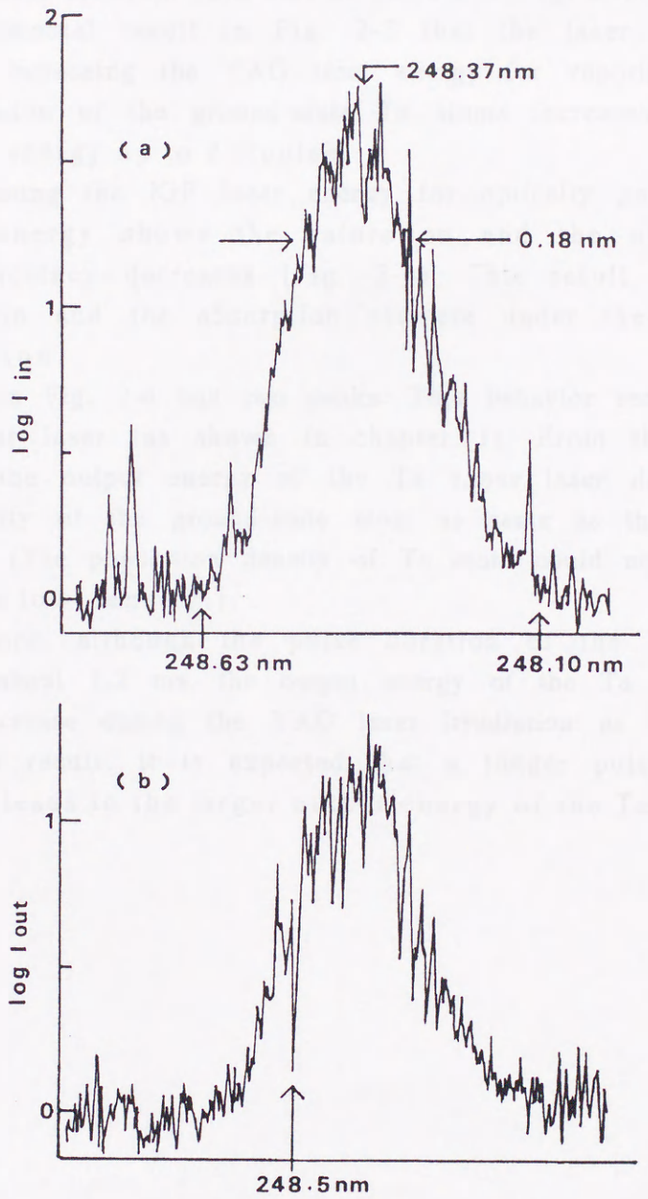

FIG. 2-8. Densitometer traces of (a)the KrF laser light and (b)the light passing through the Ta vapor.
(He buffer gas pressure:2.5 Torr, delay time:1.3 ms, YAG laser energy:2 J/pulse, KrF laser energy:2 nJ/pulse)

The spectrum of the KrF laser passing through the Ta vapor plasma has a dent at about 248.5 nm, which is the Ta absorption line as shown in Fig. 2-1, and the I_{out}/I_{in} at 248.5 nm is about 0.12. As the loss at neighboring wavelengths of the 248.5 nm line is about 33 %, the net absorption of the KrF laser by the ground-state Ta atoms is estimated to be 0.36. From the equation $I_{out} = I_{in} \cdot exp(-\beta \cdot L)$, an absorption coefficient β is calculated to be 0.46 /cm, where L is the horizontal length of the laser medium (2.2 cm) as shown in Fig. 2-7.

The experimental result in Fig. 2-5 that the laser output energy increases with increasing the YAG laser energy for vaporization suggests that the population of the ground-state Ta atoms increases linearly with the YAG laser energy up to 2 J/pulse.

With increasing the KrF laser energy for optically pumping, the Ta laser output energy shows the saturation and the optical energy conversion efficiency decreases (Fig. 2-6). This result indicates that the optical gain and the absorption saturate under the condition of strong excitation.

The curve in Fig. 2-4 has two peaks. This behavior resembles to that of an Fe vapor laser (as shown in chapter 1). From this fact, it is presumed that the output energy of the Ta vapor laser depends on the population density of the ground-state atom as same as the case of the Fe vapor laser. (The population density of Ta atom could not be measured because of it's low density.)

In this work, although the pulse duration of the YAG laser is limited within about 1.3 ms, the output energy of the Ta vapor laser is continued to increase during the YAG laser irradiation as shown in Fig. 2-4. From this result, it is expected that a longer pulse duration of the YAG laser leads to the larger output energy of the Ta laser.

CONCLUSIONS

CONCLUSIONS

New metal vapor lasers have been developed as the light source of the spectroscopic analysis in the nuclear power plant.

An Fe atom is one of important measuring objects in the nuclear power plant, because Fe atoms in materials such as a stainless steel deposit into the cooling water and they are radioactivated. The laser oscillation of Fe I atom has been first observed from optically pumped Fe vapor. The Fe vapor is produced by irradiating the Fe metal plate with the Nd:YAG laser, and Fe atoms in the vapor are optically pumped by the KrF laser. The Fe laser oscillations are obtained on three lines in ultraviolet region (299.951, 303.164 and 304.043 nm), and on two lines in visible region (532.418 and 562.455 nm). The maximum output energy of the ultraviolet Fe laser is 1.08 μJ, and that of the visible Fe laser is 135.3 nJ.

In order to elucidate the oscillation mechanisms of the Fe vapor laser, population densities of Fe atoms, the absolute gas temperature and the electron density in the vapor plasma have been measured. By using the experimental data, population densities of Fe atoms in the laser upper and lower states have been calculated with the aid of a set of rate equations. As the result, it is elucidated that the optical gain or the output power of the Fe vapor laser is dominated by not only the transition probability of the laser line but also the population of the laser lower state.

In a nuclear reactor, a concentration of Ta atoms in materials such as a niobium steel is strictly controlled, because the Ta atom has a high neutron absorption cross section. The laser oscillation of Ta I atom has also been first observed from optically pumped Ta vapor. The Ta vapor is produced by irradiating the Ta metal plate with the Nd:YAG laser, and Ta atoms in the vapor are optically pumped by the KrF laser. The Ta laser oscillations are obtained on five lines in ultraviolet region (292.519, 322.732, 328.087, 330.438 and 351.361 nm). The maximum output energy of the Ta vapor laser is 160 nJ.

The above metal vapor lasers offer light sources of various wavelengths by changing the metal plate in the same device, which are very useful as a light source of a spectroscopic analysis or a separation of metallic elements.

REFERENCES

1 P. Delobelle, Mech. Behav. Mater 6, 1, 93 (1992).

2 J. C. Danko, R. Sasaki, H. Itow, S. Iwasaki, Y. Saiga and K. Nojima, Proc. Stainl. Steels 91, 1,161 (1991).

3 R. Garnsey, Proc. 1988 JAIF Int. Conf. Water Chem. Nucl. Power Plants, 2, 333 (1988).

4 R. Riess, Proc. 1988 JAIF Int. Conf. Water Chem. Nucl. Power Plants, 1, 15 (1988).

5 W. Bilanin, D. Cubicciotti, R. L. Jones, A. J. Machiels, L. Nelson and C. J. Wood, Prog. Nucl. Energy, 20, 43 (1987).

6 P. R. Blazewicz, W. B. Whitten and J. M. Ramsey, Anal. Chem., 61, 1010 (1989).

7 J. B. Simeonsson, K. C. Ng, and J. D. Wineforder, Appl. Spectrosc., 45, 1456 (1991).

8 D. Franzke, H. Klos and A. Wokaun, Appl. Spectrosc., 46, 587 (1992).

9 M. Kusaba,N. Nakashima, Y. Izawa and C. Yamanaka, Chim. Phys. Lett., 197, 136 (1992).

10 A. Iwata, N. Nakashima, Y. Izawa and C. Yamanaka, Anal. Chim. Acta., 277, 25 (1993).

11 K. G. Manohar, K. Dasgupta, B. M. Suri and D. D. Bhawalkar, Rev. Sci. Instrum., 58, 920 (1987).

12 R. Kapoor, B. M. Suri and G. D. Saksena, J. Phys. E, 18, 930 (1985).

13 R. W. Balliett, M. Coscia and F. J. Hunkeler, J. Metals, 38, 25 (1986).

14 H. M. Ortner, P. Wilhartitz and M. Grasserbauer, Key Eng. Mater., 29, 21 (1989).

15 R. F. Hazelton, US. DOE. Rep., No.PNL-6273, 56 (1987).

16 American Society for Metals, Metals Handbook 9th Edition, 2, *Properties and Selection-Non-Ferrous Alloys and Pure Metals*, (1979).

17 W. T. Silfrast, O. R. Wood Ⅱ and J. J. Macklin, Appl. Phys. Lett., 42, 347 (1983).

18 N. D. Perry and R. C. Tobin, Appl. Phys. Lett., 45, 727 (1984).

19 K. I. Zemskov, M. A. Kazaryan, T. I. Pekhoskia and A. N. Trofimov, Sov. J. Quantum Electron., 2, 235 (1979).

20 H. Yoshida, K. Nakamura, H. Ninomiya and S. Horiguchi, Opt. Commun. 105, 133 (1994).

21 W. C. Marlow, Appl. Optics 6, 1715 (1967).

22 H. Yoshida, N. Shinoda, K. Nakamura and S. Horiguchi, Mem. Konan Univ., Sci. Ser., 37, 119 (1990).

23 W. L. Wiese, Spectrochim. Acta., 46B, 831 (1991).

24 R. E. Sturgeon, S. N. Willie and V. T. Luong, Spectrochim. Acta., 46B, 1021 (1991).

25 J. F. Alder and J. M. Mermet, Spectrochim. Acta., 28B, 421 (1973).
26 P. Yang and R. M. Barnes, Spectrochim. Acta., 44B, 1093 (1989).
27 D. Karabourniotis, E. Drakakis and B. Zacharopoulos, J. Phys. D: Appl. Phys., 25, 188 (1992).
28 M. S. Chou and T. A. Cool, J. Appl. Phys., 48, 1551 (1977).
29 M. J. Linevsky and T. W. Karras, Appl. Phys. Lett., 33, 720 (1978).
30 D. W. Trainor and S. A. Mani, Appl. Phys. Lett., 33, 31 (1978).
31 C. H. Corliss and W. R. Bozman, *Experimental Transition Probabilities for Spectral Lines of Seventy Elements* (U.S.Government Printing Office, Washington DC, 1962).
32 F. M. Phelos Ⅲ, *MIT Wavelength Table 2* (MIT Press, Cambridge, 1982).
33 C. E. Moore, *Atomic Energy Levels*, (National Bureau of standards, Washington DC, 1958).
34 M. Shimauchi, S. Karasawa and T. Miura, J. Chem. Phys., 68, 5657 (1978).
35 A. Yariv, *Quantum Electronics* (John Wiley & Sons. Inc., New York, 1975), 176.
36 C. Brechignac, Ph. Cahuzac and A. Debarre, Phys. Rev. A, 31, 2950 (1985).
37 A. Kallenbach and M. Kock, J. Phys. B, 22, 1705 (1989).
38 R. G. Caro, M. C. Gower and C. E. Webb, J. Phys. D, 15, 767 (1982).
39 M. Aden, E. Beyer, G. Herziger and H. Kunze, J. Phys. D: Appl. Phys., 25, 57 (1992).
40 C. S. Willet, *Introduction to Gas lasers: Population Inversion Mechanisms* (Pergamon, Oxford, 1974).
41 Yu. Raizer, Sov. Phys., JETP 21, 1009 (1965).
42 P. E. Nielsen, J. Appl. Phys., 46, 5401 (1975).

ACKNOWLEDGEMENTS

This work has been carried out in Shikoku Research Institute Incorporated. The author would like to thank Professor Shiro Horiguchi, for stimulating and helpful discussions. The author wish to acknowledge valuable discussions with Dr. H. Ninomiya and R. Tamaki. The author also thank the hospitality and encouragement of Professor R. Kikuchi, Professor K. Yuasa, and Professor W. Sasaki.